Hydrothermal equalibria and ore formation

Alekseyev V.A., Medvedeva L.S., Starshinova N.P. Influence of temperature gradient on equilibrium relations in quartz-water (solution) system at 300°C

V. I. Vernadsky Institute of Geochemistry and Analytical Chemistry RAS, Moscow

Abstract. Our study has shown that even small temperature gradient (0.25 °/cm) that is difficult to avoid in experiments leads to transformation of equilibrium quartz-water (solution) system into non-equilibrium one. This displays in the re-deposition of quartz from ampoule bottom onto their walls above the meniscus and in the decrease of aqueous silica concentration lower than quartz solubility. The probable mechanism causing this transformation can be combined action of the predominant evaporation at the meniscus edge and the thermal diffusion.

Key words: quartz, water, equilibrium violation, temperature gradient, thermal diffusion, predominant evaporation, meniscus edge.

Citation: Alekseyev, V.A., L.S. Medvedeva, N.P. Starshinova (2013). Influence of temperature gradient on equilibrium relations in quartz-water (solution) system at 300°C. *Vestnik ONZ RAS, 5,*

Introduction. In our previous paper [Alekseyev et al., 2012], we have revealed in some runs at 300°C the transformation of equilibrium quartz-water system into non-equilibrium one whereas in other analogous runs such transformation was not observed. In this study, we present the results of new experiments on this question and give a new explanation of the results taking into account different temperature gradients (TG) in upper and lower part of electric furnace.

Methods. The crushed natural quartz with the grain size of 10-63 μ cleaned from dust particles and the distilled water or 0.01 M solution of HF, NaF, NaOH with the mass ratio of 0.005 were placed into Au or Pt ampoule. The ampoule was hermetically sealed and heated in the autoclave at 300ºC. The filling of ampoules with solution at run temperature was 0.6, i.e. liquid and vapor phase of the water were presented. Two series of runs with water were fulfilled: 1) quartz + water and 2) quartz + water + Pt net. The net was maintained with the help of the frame made of Pt ribbon so that the meniscus at run temperature was at the middle of the net. The autoclaves were heated coupled, one on another, in the holes of Al block situated in the middle of the electric furnace with the aim to smooth temperature. The values of TG in the Al block were 0.25 and –0.16 º/cm at the level of lower and upper autoclave respectively. Positive and negative sign of the TG means that rise and decrease of temperature from below to up prevents water from mixing and promote its mixing in autoclaves respectively at the expense of buoyancy forces. After the given time at 300ºC, the autoclaves were quenched in cold water, the ampoules were opened, the solutions were filtered (the pore size was 0.05 μ), diluted with HCl solution (2%) and analyzed for silica concentration (ICP-AES and photometry). The location of secondary silica phases was determined with the help of endoscope. Then they were scraped and analyzed using X-ray diffraction, scanning electron microscopy (SEM), and BET method (specific area).

Results. In all experiments fulfilled in the upper autoclaves, the aqueous silica concentration (*m*) was not changed with time and was equal to the quartz solubility (fig. 1). The initial quartz in these experiments was always retained on the ampoule bottom and new solid phases were not formed. These data show the achievement of equilibrium in quartz-water (solution) system.

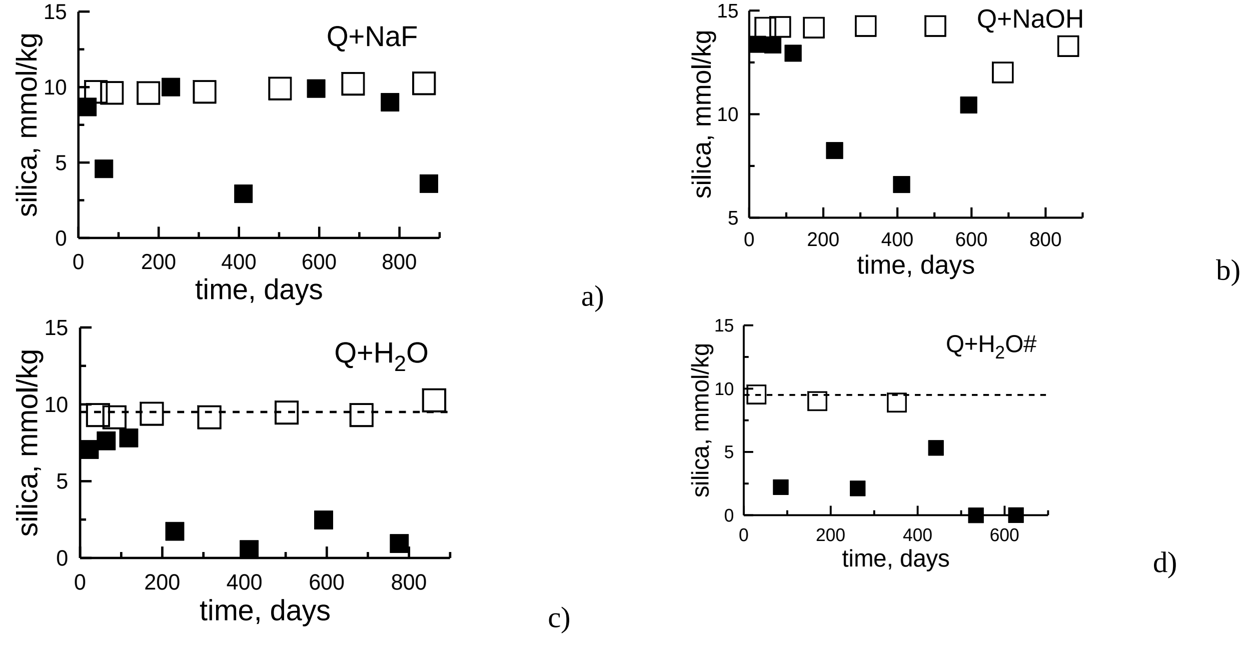

Fig. 1. Aqueous silica concentrations in quenched solutions *vs* time in the series quartz + 0.01 M NaF (a), quartz + 0.01 M NaOH (b), quartz + water (c), and quartz + water + Pt net (d). The runs were conducted in the upper autoclaves (empty symbols) with TG = -0.16 °/cm and in the lower autoclaves (filled symbols) with TG = 0.25 °/cm (the temperature rise from below upwards). The dashed lines show quartz solubility in water at 300°C [Rimstidt and Barnes, 1980].

In the series with HF, the values of *m* in the lower autoclaves were the same as in the upper ones. In the series with NaF, they were smaller in a half part of the runs in the lower autoclaves (fig. 1a). In the series with NaOH and particular with H_2O, the values of *m* were substantially smaller in all runs fulfilled in the lower autoclaves (figs. 1b, c, d). In these runs, the initial quartz was completely dissolved and new silica crusts were formed instead of it. The crusts were situated considerably above the meniscus at the run temperature at the very top of the ampoule or at the upper edge of Pt net.

In the two latest runs of the series with quartz, water, and Pr net, the value of *m* was 300 times lower than quartz solubility (table). According to X-ray diffraction data, the new-formed silica crusts in the series with water were composed with opal transforming into secondary quartz with time. The both minerals had high specific area *s* (table) owing to small crystal size of opal or small pores in the quartz crystals (fig. 2).

Discussion. We obtained new, more convincing evidence that unusual silica behavior in the lower autoclaves is not a consequence of methodical mistakes. The integrity of the ampoules was controlled by the equality of silica mass in them before and after the runs and also by the absence of silica in the space between outer ampoule walls and inner autoclave walls. The absence of quenched effect, i.e. silica precipitation from solution during quenching, was proved by the special experiments with quartz and water with high ratio of *S/M* = 1200 m^2/kg (*S* is the surface area of a mineral, *M* is the water mass) close to *S/M* values in our runs (table). Under other equal conditions (the quenching rate, the time from quenching to filtration and dilution of solution) just this quantity determines the rate of silica precipitation from solution [Rimstidt and Barnes, 1980]. In these experiments fulfilled in the upper autoclaves, the value of *m* in quenched solution was equal to the quartz solubility in water at 300ºC.

Table. The results of the longest experiments with quartz and water in the lower part of electric furnace (TG = 0.25 °/cm).

t, days	***m*, mmol/ kg**	**new solid phase**	***s*, m²/g**	***S/M*, m²/kg**	**t, days**	***m*, mmol/ kg**	**new solid phase**	***s*, m²/g**	***S/M*, m²/kg**
quartz + water					**quartz + water + Pt nets**				
410	0.58	opal-CT	109	545	84	2.25	opal-C	260	1300
591	2.51	opal-CT	95	475	261	2.15	opal-C	310	1550
775	0.98	opal-CT	190	950	441	5.35	quartz	120	600
					533	0.029	quartz	114	570
					625	0.027	quartz	78	390

Under the conditions of our experiments, quartz is a stable mineral [Dove, 1995; Klein and Hurlbut, 1993]. It has the lowest solubility in water and aqueous solutions among all silica modifications (opal, cristobalite, tridymite and so on) that are unstable and transform into quartz with time [Bettermann and Liebau, 1975; Carr and Fyfe, 1958]. The results of our runs fulfilled in the lower autoclaves contradict to the cited data and show violation of equilibrium between quartz and water (solution). The contradiction is explained by the existence of a small positive TG that prevents the water or the solution from mixing inside the ampoule. In our previous paper [Alekseyev et al., 2012], we concluded that the most probable reason that can explain these data is the predominant evaporation at the meniscus edge under the condition of temperature gradient [Panchamgam et al., 2008]. According to the hypothesis, the precipitation of secondary silica has to proceed at the same site and porous Pt nets must promote the process owing to capillary sucking.

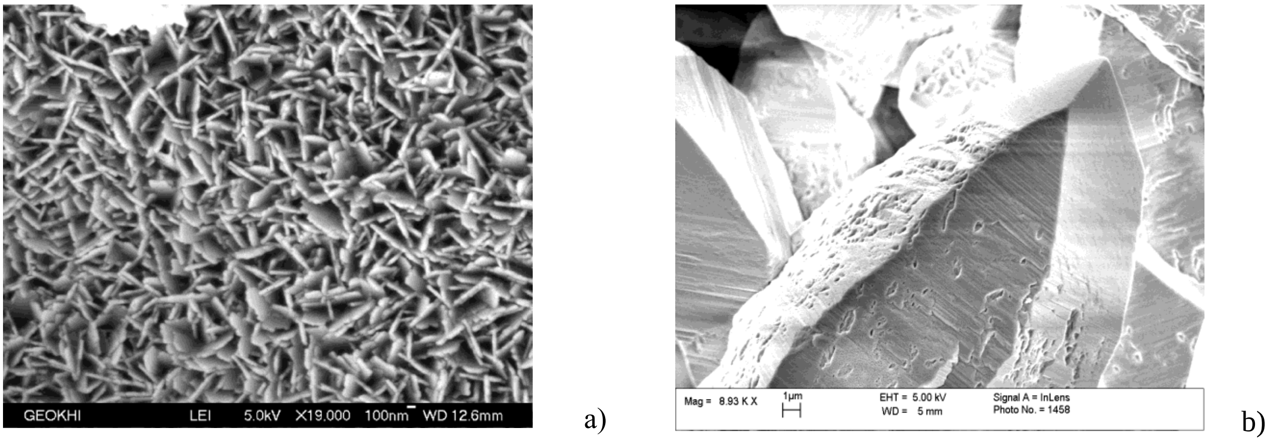

Fig. 2. SEM-photo of the crystals of secondary opal (a) and of the porous crystals of secondary quartz (b) formed on the ampoule walls above the meniscus.

However our new data contradict to this point of view. The secondary silica was not formed at the meniscus edge neither on the walls nor on the nets but was precipitated clearly above the meniscus. The alternative reason explaining our data can be thermal diffusion (Soret effect) providing with additional silica flux upwards owing to temperature gradient [Agar and Turner, 1960]. At steady state, the flux of thermal diffusion is balanced by the back-directed flux of molecular diffusion. As a result, steady profile of the concentration is formed with rise up from bottom. The profile stability is provided with the rise of temperature up from bottom, i.e. when buoyancy forces unable to cause mixing of water or solution. At the ampoule bottom, the silica concentration is lower than quartz solubility and the initial quartz is dissolved. At the ampoule top, it is higher than the solubility of not only quartz but also opal precipitating as a result. Such profiles must be two, in liquid and vapor phase of water. After complete dissolution of the initial quartz, the solution becomes depleted with silica until the silica concentration at the ampoule top falls to quartz solubility. The Soret coefficient (σ) for aqueous silica is unknown but for other aqueous species, mainly salts, it varies usually between 10^{-2} and 10^{-3} $grad^{-1}$ [Petit et al., 1986; Seyfried et al., 1985].

In our experiments, the values of σ are greater by 3-5 orders of magnitude. It is difficult to explain this difference in the frame of the hypothesis of thermal diffusion alone even if we allow the existence of higher values of TG inside autoclave by analogy with the brine inclusions [Olander et al., 1982; Pigford, 1982]. Combined action of the two processes, i.e. the predominant evaporation at the meniscus edge and the thermal diffusion is the most probable. The role of the latest process results in the supply of aqueous silica to the meniscus and the re-deposition of solid silica from the meniscus to the ampoule top through vapor with the quartz solubility of 3 ppm [Plyasunov, 2012].

Conclusion. A small temperature gradient (TG) always exists in standard electrical furnaces destined for experimental geochemical investigations and it is difficult to avoid it. We have the TG value of 0.25 °/cm in the lower part of the electric furnaces and –0.16 °/cm in their upper part. The long experiments with quartz and water and also with solutions of NaF, NaOH, and HF (0.01 M) at 300ºC (ampoule quenched method) have shown the achievement of equilibrium only at TG equal to –0.16 °/cm. At TG equal to 0.25 °/cm, the deviations from equilibrium were observed and they grew in the row HF – NaF – NaOH – H_2O. The deviations were displayed in the re-deposition of silica from the ampoule bottom onto their walls above the meniscus and in the decrease of aqueous silica concentration lower than quartz solubility. The secondary silica was represented by opal and quartz, both with high specific area owing to small crystals and pores. The obtained paradoxical data cannot be the consequence of methodical mistakes and can be explained likely by combined action of the predominant evaporation at the meniscus edge and the thermal diffusion. The results of this work offer for geochemists to pay attention to measurement and regulation of TG in all experimental investigations. It is hardly possible to avoid TG in the experiments but it is possible to exclude its influence on the experimental results placing the autoclaves into the zone with temperature decrease from below upwards, i.e. where the mixing of solution takes place. The efficacious mechanisms of fractionation revealed by us can be suitable for other matters and can have a technological meaning.

References:

1. Alexeyev, V.A., L.S. Medvedeva, N.P. Starshinova (2013). Paradoxical transformation of the equilibrium quartz–water system into an unequilibrated one. *Geochemistry International*, V. 51, №. 5, pp. 382–404.
2. Agar, J.N., J.C.R. Turner (1960). Thermal diffusion in solutions of electrolytes. *Proc. Roy. Soc. London, Ser. A*, V. 255, № 1282, pp. 307-330, doi:10.1098/rspa.1960.0070.
3. Bettermann, P., F. Liebau (1975). The transformation of amorphous silica to crystalline silica under hydrothermal conditions. *Contrib. Mineral. Petrol.*, V. 53, № 1, pp. 25-36.
4. Carr, R.M., W.S. Fyfe (1958). Some observations on the crystallization of amorphous silica. *Amer. Mineral.*, V.43, № 9-10, pp. 908-916.
5. Dove, P. M. (1995). Kinetic and thermodynamic controls on silica reactivity in weathering environments. *Rev. Mineral.*, V. 31, pp. 235-290.
6. Olander, D.R., A.J. Machiels, M. Balooch, S.K. Yagnik (1982). Thermal gradient migration of brine inclusions in synthetic alkali halide single crystals. *J. Appl. Phys.*, V. 53, № 1, pp. 669-681, doi:10.1063/1.329975.
7. Panchamgam, S. S., A. Chatterjee, J. L. Plawsky, P. C. Jr. Wayner (2008). Comprehensive experimental and theoretical study of fluid flow and heat transfer in a microscopic evaporating meniscus in a miniature heat exchanger. *Int. J. Heat Mass Transfer*., V. 51, № 21-22, pp. 5368-5379.
8. Petit, C.J., M.-H. Hwang, J.-L. Lin (1986). The Soret effect in dilute aqueous alkaline earth and nickel chloride solutions at 25ºC. *Int. J. Thermophys.*, V. 7, № 3, pp. 687-697.
9. Pigford, T.H. (1982). Migration of brine inclusions in salt. *Nucl. Techn.* V. 56, № 1, pp. 93-101.
10. Plyasunov, A.V. (2012). Thermodynamics of $Si(OH)_4$ in the vapor phase of water: Henry's and vapor–liquid distribution constants, fugacity and cross virial coefficients. *Geochim. Cosmochim. Acta*, V. 77, pp. 215-231.
11. Rimstidt, J. D., H. L. Barnes (1980). The kinetics of silica–water reactions. *Geochim. Cosmochim. Acta*, V. 44, № 11, pp. 1683-1699.
12. Seyfried, W.E. Jr., E.C. Thornton, F.L. Sayles (1985). Heat-transfer experiment in marine pelagic clay: Implication for subseabed disposal of high-level radioactive waste and contact metamorphism in the Guaymas Basin, Gulf of California. *Chem. Geol.*, V. 53, № 1-2, pp. 135-153.

Alekseyev V.A., Medvedeva L.S. Spontaneous vilolation of quartz-water chemical equilibrium: new data and revision of previous data

V. I. Vernadsky Institute of Geochemistry and Analytical Chemistry RAS, Moscow

Abstract. Our new experiments have shown that violation of quartz-water chemical equilibrium takes place in the autoclaves situated in the lower part of electric furnace only without upper autoclaves. This is explained by modification of temperature gradient (TG) along vertical and horizontal lines. The new data have brought to a different interpretation of previous data. The model was proposed to explain equilibrium violation by solution distillation as a result of preferential evaporation at the meniscus edge. The results of this work have shown that even small TG (~0.2 º/cm) can cause a formation of the ordered system with adjacent parts not able to attain equilibrium to one another.

Key words: quartz, water, equilibrium violation, temperature gradient, preferential evaporation, meniscus edge, distillation.

Citation: Alekseyev V.A., L.S. Medvedeva (2013). Spontaneous vilolation of quartz-water chemical equilibrium: new data and revision of previous data. *Vestnik ONZ RAS, 5,*

Previous investigations. In the paper [Alekseyev et al., 2013a] the earliest data have published about unusual phenomenon of transformation of equilibrium quartz-water system into non-equilibrium one at 300ºC. This phenomenon revealed itself in the lowering of aqueous silica concentration (m_{sil}) below quartz solubility and in the re-crystallization of silica from ampoule bottom onto their walls above the water meniscus as opal. From some considered hypothesis explaining this phenomenon, the most probable is the hypothesis of preferential evaporation at the meniscus edge under temperature gradient (TG). The long runs (up to 600 days) where the phenomenon was present alternated with the runs where the phenomenon was absent. The next experiments [Alekseyev et al., 2011] have explained this inconstancy. The point is that experiments were conducted in autoclaves placed in electric furnace in pairs, one above another (Fig. 1). The phenomenon proved to reveal itself only in the lower autoclaves where temperature rises up from the bottom. The only exception was the longest experiment in the lower autoclave with m_{sil} value equal to quartz solubility. Its peculiarity was that this lower autoclave was took out shortly after the removal of upper autoclave. Owing to this reason, we proposed that the phenomenon of m_{sil} decrease in the lower autoclaves reveals itself only when upper autoclaves are absent. In this case the time dependence of m_{sil} takes the shape shown in Fig. 2 and the overall process duration becomes shorter by an order of magnitude.

New investigations. To prove this assumption, we conducted short duration experiments without quartz but with water saturated with silica relative to quartz. These experiments are more sensitive to studied phenomenon than the experiments with quartz and water as silica decrease is not compensated by dissolution of quartz excess. The value of m_{sil} in quenched solutions was determined by photometric method using ammonium molibdate with accuracy of 5 rel. %. These experiments have confirmed our assumption. When the upper and lower autoclaves were pulled out simultaneously, m_{sil} values in the lower autoclaves were not reduced at various inclinations of autoclaves in the furnace and ampoules in autoclaves (Fig. 3, left part). When the upper autoclaves were absent, m_{sil} values in the lower autoclaves were smaller (Fig. 3, right part) and minimum m_{sil} values were in the vertical autoclaves. Analogous experiments with HF solution (0.01 m) also have shown the decrease in m_{sil}. This is contradict to the previous experiments without such decrease [Alekseyev et al., 2013b]. This contradiction can be explained that earlier four ampoules were successively placed into one autoclave: at first with water, then with solutions of NaOH, NaF, and HF. The reduction of the phenomenon of m_{sil} decrease was observed in the same sequence and can be the result of not the influence of solution composition but the change in TG along the autoclave height (the last ampoule with HF was situated much higher than the first ampoule with water).

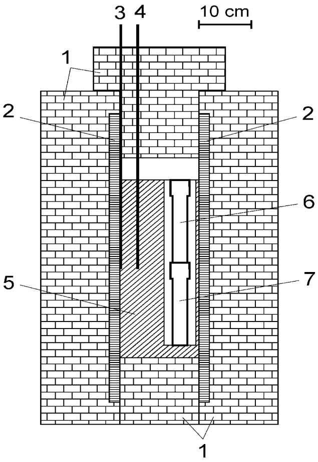

Fig. 1. Longitudinal section of vertical tubular electric furnace.
1 – thermal isolation, 2 – heater, 3 – regulating thermocouple, 4 – showing thermocouple, 5 – aluminum block with three hollows for autoclaves (destined for temperature smoothing), 6 – upper autoclave, 7 – lower autoclave (autoclaves can deviate from vertical axis up to 10º). Hermetic gold or platinum ampoules with water and quartz were placed in autoclaves. At run temperature, the filling of ampoules with water was ~0.7, i.e. the water was present in the form of liquid and vapor.

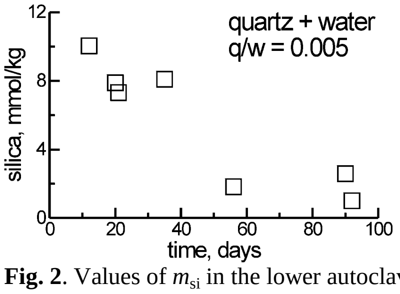

Fig. 2. Values of m_{si} in the lower autoclaves vs. time of their exposition at 300ºC without upper autoclaves.

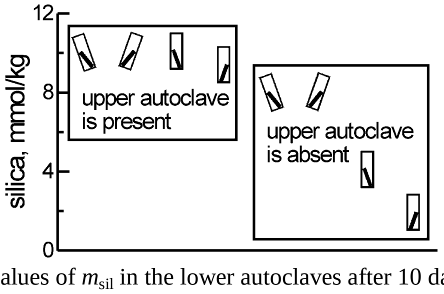

Fig. 3. Values of m_{sil} in the lower autoclaves after 10 days at 300ºC. The initial m_{si} value is 10 mmol/kg.

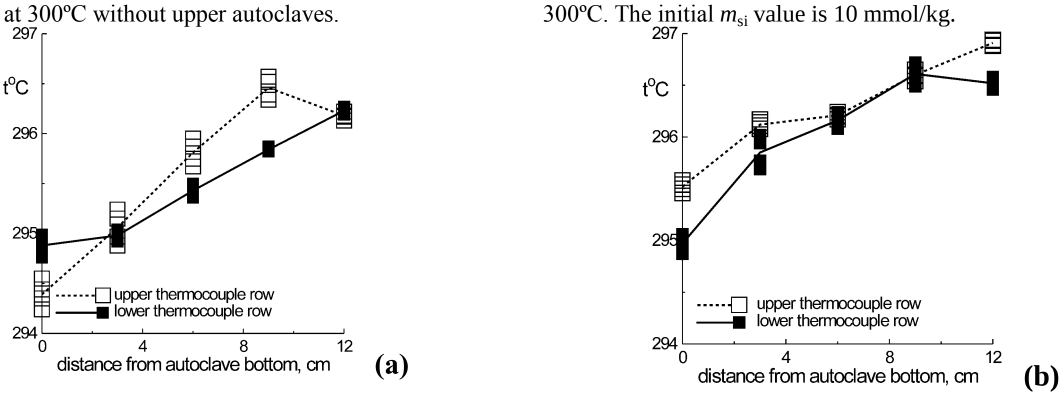

Fig. 4. Temperature on the surface of the lower inclined autoclave: a – upper autoclave is present, b – upper autoclave is absent.

Temperature gradient (TG) was measured at the minimum distance from the reaction zone (3 mm), i.e. on the autoclave surface. Temperature was measured using 10 chromel-alumel thermocouples with hot ends situated on two opposite sides of autoclave, five in each line. Temperature was measured several times with different thermocouples at different locations and this was alternated with measurements of corrections for thermocouples when their hot ends were coincided. The standard error of the measurements was 0.2º. These measurements have shown that up from the bottom the temperature decreases on the surface of upper autoclave and increases on the surface of lower autoclave. It is agree with our previous TG measurements in the aluminum block where autoclaves were inserted [Alekseyev et al., 2013a]. But now new details of TG measurements have appeared. In particular, the divergence of temperatures between thermocouple lines on Fig. 4a gives evidence of the presence of appreciable horizontal TG. The extraction of upper autoclaves leads to another distribution of horizontal TG (Fig. 4b). The values of TG at autoclave bottom where ampoules were situated are shown in Fig. 5. It is seen from this figure that positive horizontal TG assists the phenomenon display.

Discussion. We suppose that the probable mechanism of the influence of TG on m_{sil} is the preferential evaporation at the meniscus edge [Panchamgam et al., 2008] dependent on the direction and quantity of TG. As a result, distillation takes place, i.e. the decrease of m_{sil} in liquid water up to quartz solubility in vapor water equal to ~50 μmol/kg [Plyasunov, 2012]. This value is close to the minimum m_{sil} values (30 μmol/kg) obtained by us in the longest experiments [Alekseyev et al., 2011; 2013a] which confirms the proposed mechanism. The distillation model is following. The more concentrated solution flows out of a reservoir and the less concentrated solution flows into the reservoir with the same rate. In the reservoir, the solution has homogeneous concentration as a result of mixing. The modeling results have shown the typical shape of the kinetic curves (Fig. 6). In future, experimental verification of the model is proposed.

The results of this work have shown that even small TG (~0.2 º/cm) can cause the formation of an ordered system with neighboring parts that cannot come to equilibrium to one another. This circumstance can cause the distortion of the results of kinetic and equilibrium experiments with various minerals and aqueous solutions.

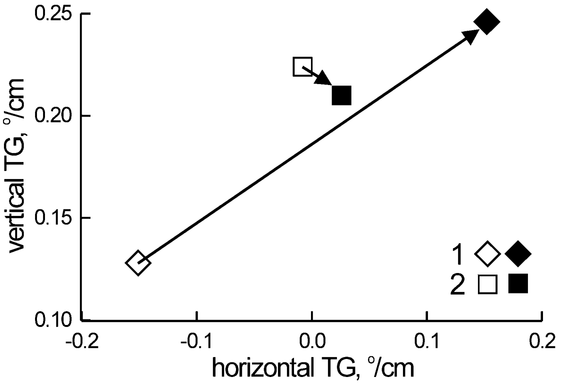

Fig. 5. Temperature gradients (TG) at the bottom of the lower inclined (1) and vertical (2) autoclaves. Empty symbols denote the absence of the phenomenon, filled symbols denote its presence. Arrows show gradient change after removing upper autoclaves.

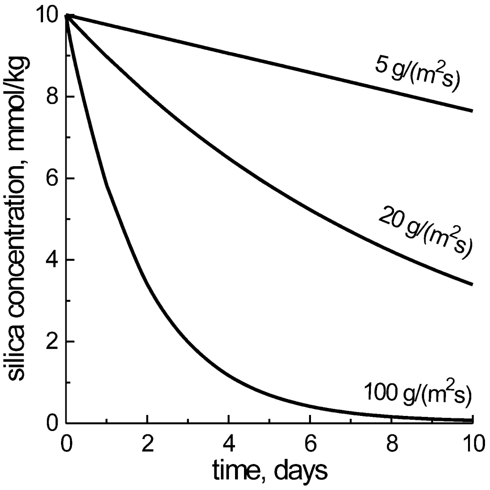

Fig. 6. Modeling results of m_{sil} dependence on time for various rates of preferential evaporation at the meniscus edge with ampoule diameter of 1 cm and water mass of 1 g.

References:

1. Alekseyev V.A., L.S. Medvedeva, N.P. Starshinova (2011). Transformation of equilibrium quartz-water system into non-equilibrium one under a small temperature gradient. *Vestnik Otdelenia nauk o Zemle RAN*, V. 3, NZ6005, doi:10.2205/2011NZ000135, 2011. URL: http://onznews.wdcb.ru/publications/v03/asempg11en/2011NZ000135.pdf
2. Alexeyev V.A., L.S. Medvedeva, N.P. Starshinova (2013a). Paradoxical transformation of the equilibrium quartz–water system into an unequilibrated one. *Geochemistry International*,V. 51, №. 5, pp. 382–404.
3. Alekseyev V.A., L.S. Medvedeva, N.P. Starshinova (2013b). Influence of temperature gradient on equilibrium relations in quartz-water (solution) system at 300°C. *Vestnik Otdelenia nauk o Zemle RAN*, V. 5, (this issue).
4. Panchamgam S.S., A. Chatterjee, J.L. Plawsky, P.C.Jr. Wayner (2008). Comprehensive experimental and theoretical study of fluid flow and heat transfer in a microscopic evaporating meniscus in a miniature heat exchanger. *Int. J. Heat Mass Transfer*., V. 51, № 21-22, pp. 5368-5379.
5. Plyasunov A.V. (2012). Thermodynamics of $Si(OH)_4$ in the vapor phase of water: Henry's and vapor–liquid distribution constants, fugacity and cross virial coefficients. *Geochim. Cosmochim. Acta,* V. 77, pp. 215-231.

Aksyuk A.M., Korzhinskaya V.S., Konyshev A.A. Experimental investigation of albite and microcline solubilitys in hf solutions at T = 400º, 500ºC and P = 1000 bar

Institute of Experimental Mineralogy RAS, Chernogolovka

Abstract. the paper presents the results for the solubility of natural albite and microcline minerals in HF solutions with concentrations from 10^{-6} m up to 2 m at T = 400º, 500ºC and P = 1000 bar. The solubility monotonously increases in the area of low HF concentration (10^{-6}-10^{-2} m), then it abruptly grows with the increase of the initial HF concentration by about 3 order. The temperature influence in the range of 400-500ºC is significantly less.

Key words: experiment, albite, microcline, solubility, fluorine.

Citation: Aksyuk A.M., V.S. Korzhinskaya, A.A. Konyshev (2013), the Experimental investigation of albite and microcline solubility in HF solutions at T=400°-500°C and P=1000 bar. Bulletin ONZ RAS, (doi:

For the assessment of the concentration levels for the components such as Na, K, Al, Si, Ta, Nb, Be in the natural fluids at the formation of greisen and hydrothermal ores, there are important solubility of rare metal deposits minerals: feldspar (albite, microcline), topaz, Ta-Nb-containing and beryllium ones (beryl, chrysoberyl, phenakite) in fluoride solutions. The albitite and feldspatite bodies met in the granite domes on fluorite deposits of Primorye (Russian Far East), the formation of which is connected, in our data, with high fluoride (0.1 m HF and above) fluids. In the literature there are some experimental studies on the behavior of albite, microcline in HF solutions [Zaraisky, Stoyanovskaya, Tikhomirova, 1999], but its covers hydrothermal area not wide enough. It is necessary to expand the study in temperature, pressure, oxidation-reduction conditions and concentrations of fluoride.

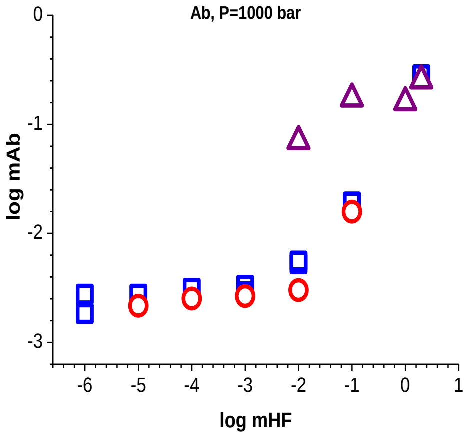

Fig. 1. Solubility of albite in HF solutions for P = 1000 bar: squares is at 500°C (by the method of weight loss crystal); circles is at 500°C (data of the chemical analysis); triangles is at 400°C (by the method of weight loss crystal)

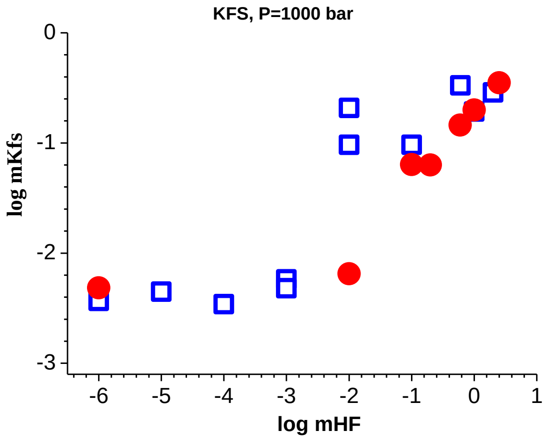

Fig. 2. Solubility of Kfs in HF solutions for P = 1000 bar: circles is at temperature 400°C; squares is at 500°C

We are conducting an experimental study for the solubility of natural albite and microcline minerals in HF solutions with concentrations from 10^{-6} m up to 2 m at T = 400°, 500°C and P = 1000 bar The selected range of the HF concentrations correspond to an actual range of fluoride in natural postmagmatic fluids on rare metal deposits, connected with granite. According to the data received on the basis of experimental calibrated mica geofluorimeter [Aksyuk, 2002] on the гидротермальном stage of the of ore-magmatic systems evolution the HF concentration in seceding from the granite melt water fluids can be up to 1 - 2 mol/kg H_2O. Experiments with duration of 15 - 20 days spent in closed platinum ampoules at hydrothermal high pressure exoclave apparatus. Natural crystals of sugar-like albite (cleavelandite), which come near to the composition of the net albite $(Na_{0.94}K_{0.009}Ca_{0.005})Al_{1.01}Si_{2.98}O_8$ (microprobe analysis) were selected. On a **photo 1** shows the crystal cleavelandite, and the **photo 2** there are the crystal microcline with perthitic intergrowths of albite, with the average composition $(K_{0.74}Na_{0.27}Ca_{0.006})Al_{1.01}Si_{2.98}O_8$ or $Ort_{0.74}Ab_{0.27}$. Fragments were cut of them and used in the experiments. They have the size of about 3-5 mm and weight of 0.1-0.2 gram. Solubility of albite and microcline studied weight loss method of single crystal with an accuracy of weighing ±0.00001 grams. For some experiments of albite solutions were discussed as well chemical methods: the Si, Al, Na. New phase of solid sample studied for a microprobe electronic CamScan MV2300 (VEGA TS 5130MM), x-ray and optical methods in order to control congruent or incongruent dissolution of minerals and to determine the chemical composition. Part of the experiments to microcline held on two ampoula methodology, when the crystal was placed in the open platinum cylinder of the 5 mm diameter, and she was in platinum sealed ampoule with a HF solution. The amount of the solution has 1 ml in external ampoule with a diameter of 10 mm. It is established, that albite and microcline dissolved in HF incongruent with the major transition in the solution of silicon on its stoichiometric content in the mineral.

In Fig. 1 and 2 show the concentration dependence of the mineral solubility of albite (**Fig. 1**) and microcline (**Fig. 2**). Total solubility of both minerals monotonously increases in the area of low concentration of HF (10^{-6}-10^{-2} m), then she abruptly grows with the increase of the initial concentration of HF: approximately 3 order. The temperature influence is significantly less on the range of 400-500°C. Total solubility of albite at T = 500°C monotonically increases from $2.77*10^{-3}$ up to 5.32*10-^{3} mol/kg H_2O with the increase in the concentration of HF from 10^{-6} to 10^{-2} m, and then sharply increases up to $1.94*10^{-2}$ mol/kg H_2O in solution 0,1m HF. With this increase in the solubility of albite is not only due to growth of the silica concentration, whose contribution to the total solubility of albite greatest, but also due to the transition in the solution of Al and Na. Discovered in experiments with a solution of 0.1 m HF exceeding concentration of SiO_2 almost an order of magnitude above the saturation of quartz, apparently, is connected with the formation of amorphous silica by acid decomposition of albite. At the same time, at lower concentrations HF solution remains under saturated on SiO_2 respect to quartz. In the area of high HF concentrations (1m - 2m), a sharp increase of solubility of albite to 0.285 mol/kg H_2O with the formation of new phases: quartz (Qtz) and phase $Na_5Al_3F_{14}$, the relevant mineral chiolite, which is a cryptocrystalline units of white color (crystals up to 1 mm), reminiscent of lumps of snow with pearly luster and tetragonal symmetry. Solubility of albite at 500°C, calculated by the data of chemical analysis, on average slightly lower than that determined by the method of weight loss crystal, which can be attributed to the loss of part of the substances in the precipitation process of hardening. Solubility of albite at T = 400°C and P = 1000 bar on the procedure above for the HF concentrations 0.01m and 0.1m, and in the area of high concentrations of HF (1m and 2m) it coincides with the solubility of the mineral at 500°C.

Solubility of microcline (see Fig. 2) for the temperature of 500°C is on half order above the solubility of albite. The interpretation of experimental results is hampered by the presence in the microcline samples a perthite intergrowths of albite in the amount of about 27 mol. %. Total solubility, defined under the weight loss of the crystal, is $4.84*10^{-3}$ mol/kg H_2O in pure water and then monotonically increases to $6.47*10^{-3}$ mol/kg H_2O in the solution of 0.01 m HF. More sharply, it increased to 0.288 mol/kg H_2O in 2 m HF. As albite, microcline dissolves incongruently with priority, on stoichiometry, the transition in the solution of silica in comparison with Al and K, however, the concentration of SiO_2 in the solution does not reach the level of saturation of quartz, remaining in 2-3 times lower. In the solid sample quartz appears only in the 2 m HF (by the data of x-ray phase analysis). In addition, 1m and 2 m HF firm in the sample there is a new phase in the form of needle-like crystals, shown in the **photo 3**.

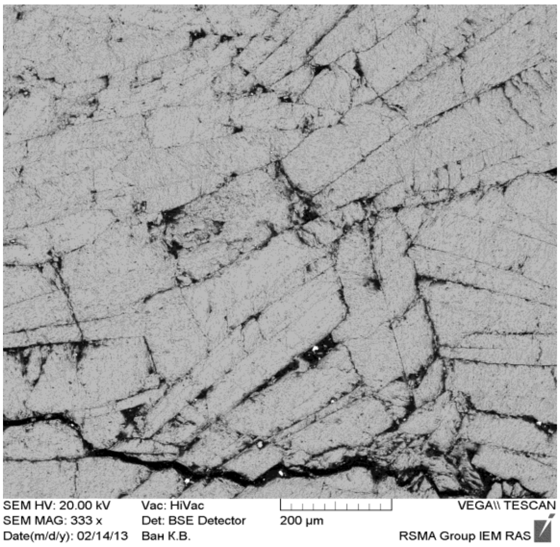

Photo. 1 Crystal albite (cleavelandite) **Photo. 2** Crystal microcline ($Ort_{0.74}Ab_{0.27}$)

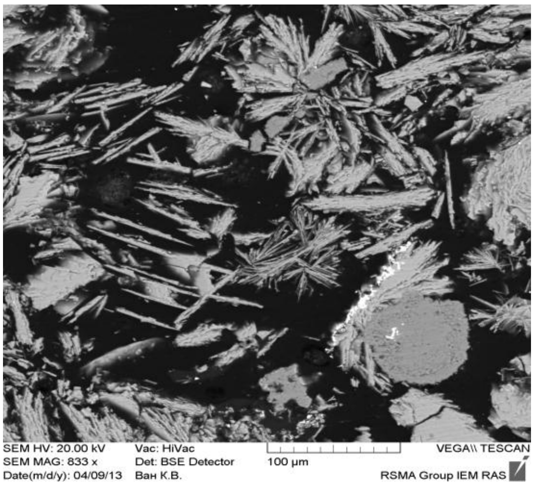

Photo 3. Crystals, formed upon the dissolution of microcline in 2 m HF (T = 500°C, P=1 kbar)

Data analysis on a microprobe showed that needle crystals represent the connection with the formula $K_2NaAl_3F_{12}$, where a part of the fluorine replaced with oxygen. Rounded spot corresponds to amorphous silica. For T = 400°C picture solubility are similar, from which it can be concluded that the impact of temperature for microcline slightly.

Studies and obtained preliminary results have shown that in conditions of moderate F-containing fluid the albite and microcline may dissolve and be transported by hydrothermal solutions, in amounts not less than quartz.

Acknowledgements: The work was done with the financial support of the ONZ-2 Program.

References:

1. Zaraisky, G.P., F.M. Stoyanovskaya, V.I. Tikhomirova (1999). Investigation of albite solubility in HF solutions at T=500°C and P=1 kbar. *Experiment in Geosciences*, V. 8, n 1, pp. 42-44.
2. Aksyuk, A.M. (2002). Experimentally calibrated geofluorimetrs and mode of fluoride in granite fluids. *Petrology*, V. 10, n 6, pp. 630-644. (in Russian)

Alekhin[1] Yu.V., Makarova[1]M.A., Karaseva[2]O.N., Mamedov[1]V.I., Poukhov[1] V.V. Experimental study the migration, adsorption and precipitation of microcomponents in lateritic airing crusts

[1]Geological faculty of Moscow State University
[2]Institute of Experimental Mineralogy RAS

Abstract. In a vertical cross section of bauxite laterite airing crust on aluminosilicate parent rocks commonly observed lithological, mineralogical and geochemical zonation sequence. The reasons for them to improve microelement is insufficiently studied. Before the experiments was previously defined trace element composition of bauxite profile. At a lateritic hyper genesis the removal trend is typical for the vast majority of the impurity elements. The steady tendency to accumulation in a lateritic cover is found by a number of rare elements, in particular: Ta, Nb, Ga, Ge. The samples of a bauxite profile rocks (bauxites and ferruterous laterites) were used in experimental works on studying dynamic the adsorptive and deposition processes. Studying of relative mobility of microelements was carried out by a method of multielement synthetic solution filtration with identical concentration of all elements (at level 100 ppb) at preset values pH 3 and 6 through a thin layer membrane with the characteristic size of particles from 1 to 5 micron, created of a bauxite rocks suspension. By the calculations of interphase interaction coefficients of solution and membrane material and extraction coefficients of initial elements from a membrane the rows of elements differential mobility, as extent of each of them participation in adsorptive and desorption processes are shown. Results of experiments will well be agreement with results of mineral composition determination and the impurity elements content in bauxites and accompanying rocks down on a cross section.

Key words: lateritic airing crusts, zonation rows of microelements, coefficient of interphase interaction, migration ability.

References: Alekhin Yu.V., M.A. Makarova, O.N. Karaseva, V.I. Mamedov, V.V. Poukhov (2013). Studying of migration, adsorption and sedimentation of microcomponents in lateritic airing crusts. Bulletin ONZ RAS

Researches of multicomponent migration regularities in modern lateritic airing crusts, being accompanied the adsorption capture of microelements on a new mineral phases surface is the key to understanding of the reasons of their zone structure and redistribution macro - and microcomponents.

The warm atmospheric water, the dissolved carbonic acid and being formed at vegetation destruction humic and carbonic acids are the main reagents and transporting agents which lead to chemical transformation of a parent substratum minerals and carrying out of soluble elements and redistribution in a profile of airing of not enough soluble elements and microcomponents.

In a vertical cross section of bauxite bearing lateritic airing crusts on aluminosilicate parent rocks lithological, mineralogical and geochemical zonal distribution with the certain sequence which reasons concerning microelements are insufficiently studied [Mamedov 2009, 2010] is usually observed.

Process of the microelements adsorptive-sedimentation removal on bauxite phases carriers as on a dynamic membranes material, is an experimental object of researches at the studying the fundamental mechanisms operating regularities of rare and dispersion elements concentrating in fracture and pore space at a mass transfer. Thus natural ranks of microelements zonal distribution can become a basis for criteria development of search of the most productive thicknesses of bauxite deposits.

The rocks examples of bauxite bearing profile (bauxites and ferruterous laterites) were used in experimental works on studying dynamic the adsorptive-sedimentation processes. Before experiments the mineral and microelement structure of a bauxite bearing profile previously was defined. From definitions of mineral structure follows that the main minerals of alumina in bauxites and ferruterous rocks accompanying them are gibbsite and boehmite. The iron minerals are goethite (alyumogetit) and hematite, which contained different ratios of the vast majority of the analyzed samples.

The removal trend at lateritic hypergenesis is typical for most elements - impurities. The alkaline earths (Ca, Mg) are actively taken out from a lateritic cover. Their content in the top of the laterite cover reduced by tens - first hundreds of times in relation to the native rock substrate. The alkaline metals are very unstable in a laterite cover. The contents of Li, Na, K, Rb, Cs decreased ten times compared to the native rock substrate. To the elements experiencing active carrying out which concentration decrease at 5-20 time, belong: Be, Co, Ni, Sr. To the elements experiencing insignificant carrying out which concentration decrease by 1.5-4 times, belong first of all: P, Mn, Cu.

Strong tendency to accumulate in the lateritic cover reveals a number of trace elements, particularly Ga. The contents of all elements is steadily increasing by 3-6 times. Similarly radioactive elements – U and Th (contents increase by 1.5-4 times) behave. Tend to accumulate in lateritic cover V and Bi (increase their concentration by 2-4 times). Insignificant accumulation in a lateritic cover is observed for lead. Lanthanides are rather inert at lateritic hypergenesis. As a rule, their contents in a lateritic cover in relation to a native substratum slightly decreases (by 1.3-2 times), or at all remains almost invariable.

The experimental studying of relative mobility of microelements was carried out by a method of a consecutive filtration of water and multielement synthetic solution through a thin layer membrane. Dynamic membrane material considered by us as an adsorptive-sedimentation chromatographic column. As the membrane material were used ferruterous sedimentation isolated fractions of laterite base surface (depth interval 6-7 m) and bauxite (depth interval 1-3 m) up to 5 microns. Through the created membrane consistently filtered: the distilled water and multielement standard solution 68B Solution A (High-Purity Standards) with identical concentration of elements Al, As, Ba, Be, Bi, B, Cd, Ca, Ce, Cs, Cr, Co, Cu, Dy, Er, Eu, Gd, Ga, Ho, In, Fe, La, Pb, Li, Lu, Mg, Mn, Nd, Ni, P, K, Pr, Re, Rb, Sm, Sc, Se, Na, Sr, Tb, Tl, Th, Tm, U, V, Yb, Y, Zn at the level of 100 µg/ml at predetermined values pH 3 (ferruterous laterites) and 6 (bauxites). The total content of the chemical elements in the solutions were determined by ICP-MS method. During experiments values pH and concentration of elements in the initial solutions used for a filtration, and in series of the received filtrates were defined.

By calculations of interphase interaction coefficient of solution and a material of a membrane extent of participation of each element in adsorption and desorption processes is shown. coefficients of interfacial interaction in time current point were calculated as the

$$R' = (C_{filtration} - C_{original})VN^{-1}m^{-1},$$

and their integral values

$$R'_{\Sigma} = \Sigma((C_{filtration} - C_{original})V)N^{-1}m^{-1},$$

here $C_{original}$ - element concentration in the solution before filtration, µg/l; $C_{filtration}$ - element concentration in the solution after filtration, µg/l; V - volume of the solution was filtered through a membrane, liters; N - content of a chemical element in the sample, µg/kg; m – weight of a laterite sample in the membrane.

The coefficient of interphase interaction of R′ reflects participation of each element of a membrane in chemical reactions with used multielement solution at the moment time, as a share from its general receipt with a filtrant. At domination of extraction processes from a material of a membrane is $R'>0$. At prevalence of processes of adsorption of an element on membrane is $R'<0$. The basis for calculations of integrated coefficients are representations that in chromatographic processes initial adsorptive accumulation of each element by sample is naturally replaced by its desorption as a result of an ionic exchange for such macro components of solution as Na, K, Ca, Mg, and also with more strongly occluded microcomponents. Thereof the limit steady state in system isn't reached [Alekhin 2011], for a general characteristic of processes of adsorption – desorption and absorption – extraction of chemical elements in experimental conditions can compare integrated (i.e. residual) indicators of their interaction to a material of a membrane [Alekhin 2012]. The more actively adsorption of chemical elements on a membrane, the weaker them migratory ability proceeded. Adsorption prevalence (and absorption at processes of reactionary interaction and sedimentation) of chemical elements by a membrane characterize by value $R'_{\sum}<0$, and a desorption (and extractions at dissolution) of elements characterize by value $R'_{\sum}>0$. Only simultaneous accounting of these processes and number of values $R'_{\sum}$ and R' allows to compare on an objective basis distinctions in mobility at filtering various on composition of initial solutions (water, as analog of a meteoric precipitation, and multielement standard solution) through a material of the separate horizons of lateritic airing crusts. Filtering of originally aggressive solutions and domination of adsorption – desorption or dissolution – sedimentation processes first of all are defined by acidity of solutions and initial concentration of microelements. In this regard the use of various initial solutions, including solution with identical concentration at once many elements, has undoubted advantage, - quantities of microelements entered with solution, as a rule, is significant more them mobile contents in a material of columns according to washing away by the distilled water. The recent data are used by us at a choice of working concentration of multielement experimental solution so that at the subsequent stage of filtering of this solution the contribution from dissolution of microelements from matrix phases was insignificant. Data in rows of mobility in the distilled water have also independent value, characterizing the initial stages of interaction with an atmospheric precipitation. They differ also by stability of the microelements majority extraction in filtering process, allow to eliminate the absorbed complex.

We will stop on the coefficients received for a case of a filtration of multielement solution - the standard at different values pH in more detail. First of all, at pH = 3 there is a considerable carrying out of Al owing to gibbsite dissolution.

For elements of iron group (Fe, Mn, Ni, Co) at pH 3 are characteristic insignificant negative values R' while at pH 6 for Ni and Co desorption processes prevail in process of receipt of new portions of a filtrate to what positive values R' (fig. 1) testify.

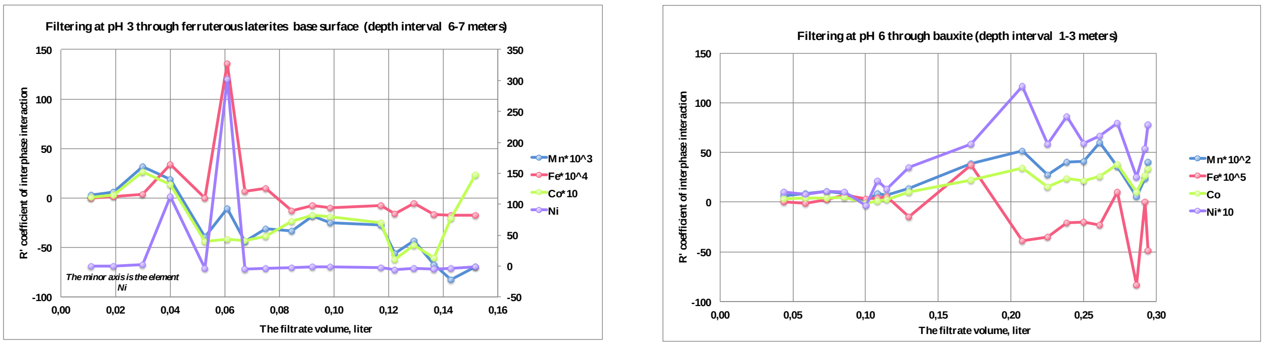

Fig. 1. Dependence of interphase interaction coefficient on filtrate volume at values pH 3 and 6.

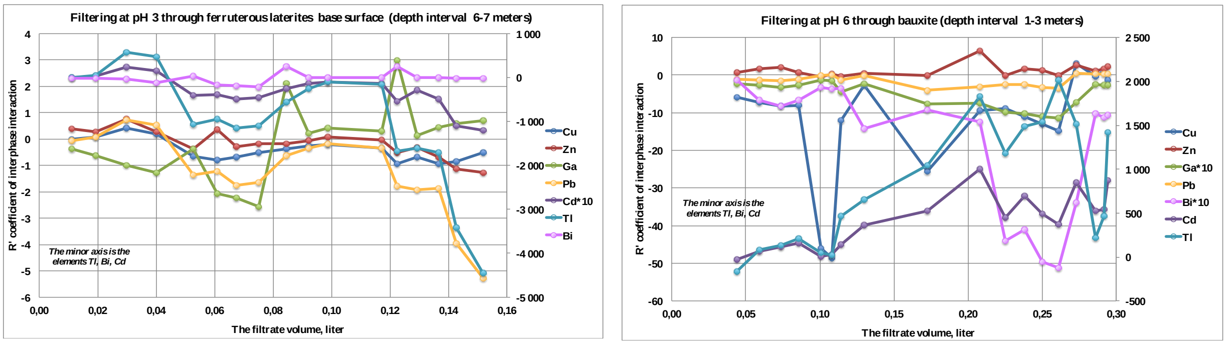

Fig. 2. Dependence of interphase interaction coefficient on filtrate volume at values pH 3 and 6.

The calculated coefficients of R' (fig. 2) for chalcophile elements (Cu, Zn, Pb and Ga) in experiments at pH 3 have values close to 0 that speaks about insignificant participation in adsorption and desorption processes at the set mode of experiment. R' for Bi, Cd, Tl have high negative values, therefore, are absorbed by a membrane material. At pH 6 high positive sizes R' for Cd and Tl testify to prevalence of a desorption of these elements while Cu is adsorbed on a membrane (fig. 2).

For microelements of lithophilous group insignificant relatives to 0 coefficients of interphase interaction are characteristic at pH 3, except for Rb, Cs, U – for these elements R´ negative, i.e. processes of adsorption are prevailing for these elements. At pH the 6 calculation of R´ for the majority of elements characterizes insignificant participation in adsorption and desorption, except for Cs which has high positive values (fig. 3).

For microelements of lithophilous group insignificant relatives to 0 coefficients of interphase interaction are characteristic at pH 3, except for Rb, Cs, U – for these elements *R′* negative, i.e. processes of adsorption are prevailing for these elements. At pH the 6 calculation of *R′* for the majority of elements characterizes insignificant participation in adsorption and desorption, except for Cs which has high positive values (fig. 4).

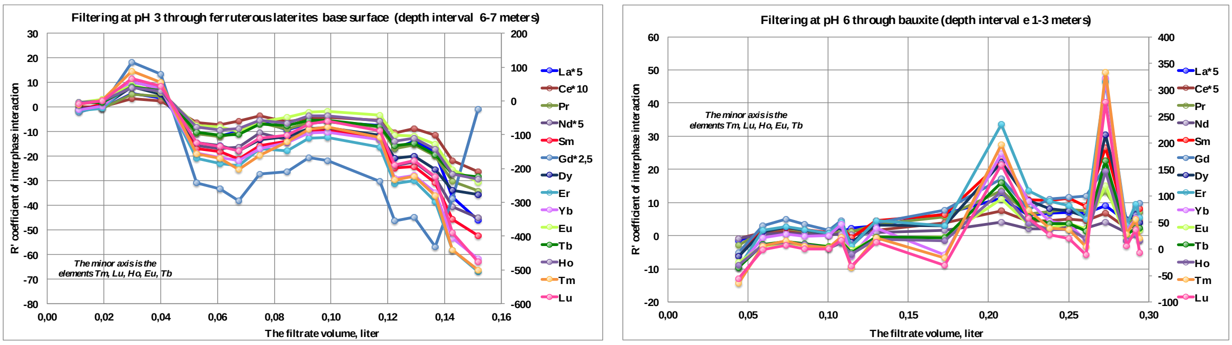

Fig. 3. Dependence of interphase interaction coefficient on filtrate volume at values pH 3 and 6.

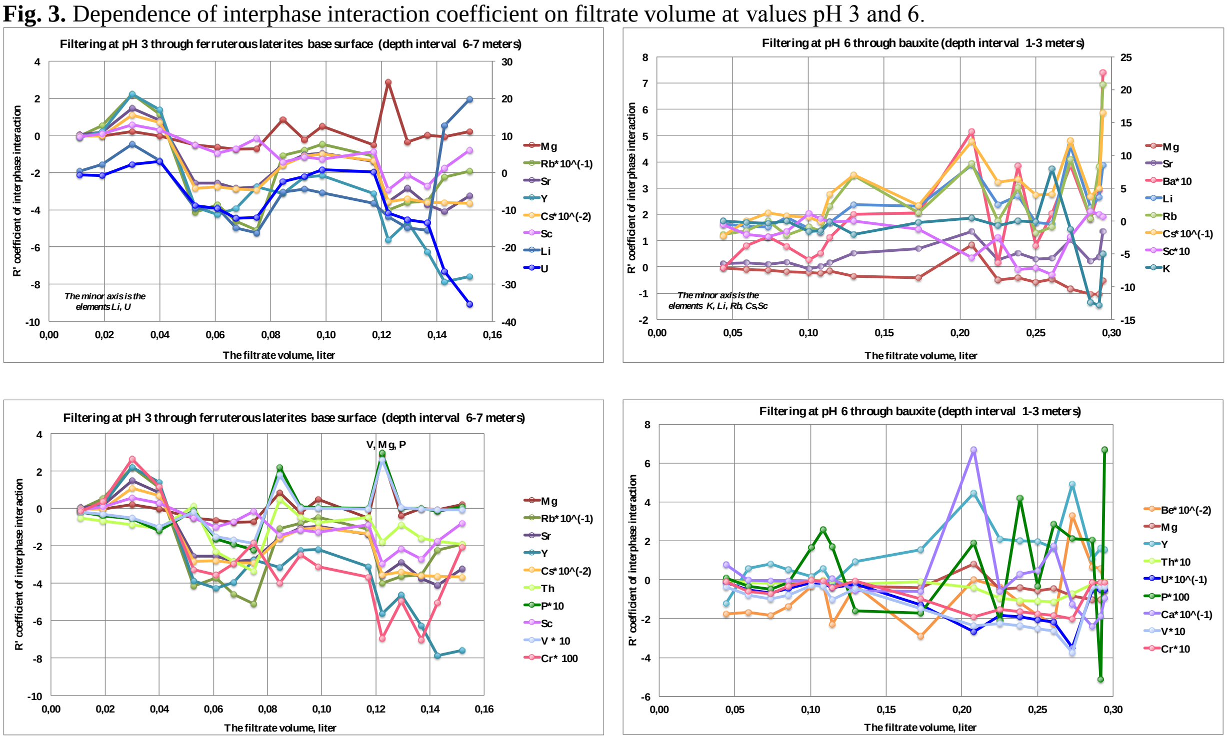

Fig. 4. Dependence of interphase interaction coefficient on filtrate volume at values pH 3 and 6.

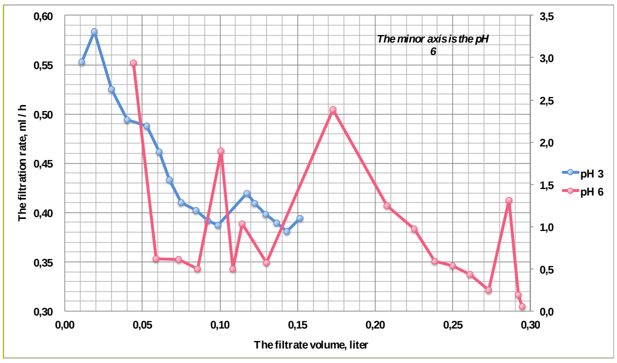

Fig. 5. Dependence filtration speed from the volume of the filtered solution.

The observed fluctuations in the values of the interfacial interaction coefficients (Fig. 1 - 4) in the course of the experiment due to variability of filtration rate and delay the pace of re-deposition of the matrix phase. At the dramatic increase in the rate of a filtration in system (fig. 5) it isn't reached a full reequilibration and there is a sporadic washing away of elements from a membrane in a filtrate. Instability and fluctuations in the first points, especially for a case at pH 3, are also connected with a transitional mode from a water filtration to a filtration of multielement standard solution when on a membrane aggressive solution with high concentration of elements moves.

With the help of calculations of integrated interphase interaction coefficients of solution and a membrane material we show rows of elements differential mobility (tab. 1, tab. 2), as extent of participation of each of them in adsorptive and desorption processes. The difference of the calculated integrated coefficients of interphase interaction for a case of a filtration of water (R´ Σ_{water}) and a filtration of standard multielement solution (R´ Σ_{st}) shows insignificance of coefficients of interphase interaction at a water filtration for the majority of elements.

Table 1. Differential mobility elements rows for filtration at pH 6 through bauxite (depth interval 1-3 meters).

$R'_{\Sigma\text{вода}}$	Cs	Co	Y	Tm	Lu	Bi	K	Cd	Tb	Ho	Eu	Cu	Mg	Li	Er	Yb	Dy	P	Sm	Gd	U
	-2,71	-1,89	-1,76	-1,72	-1,56	-1,21	-1,13	-0,89	-0,81	-0,81	-0,63	-0,44	-0,38	-0,30	-0,28	-0,23	-0,16	-0,14	-0,14	-0,13	-0,12
$R'_{\Sigma\text{ст-т}}$	Be	Cu	U	Bi	Pb	Ga	Mg	Sc	V	Cr	Th	P	Ba	Mn	Sr	Ce	Ca	La	Zn	Y	Nd
	-1 430	-219	-197	-32,2	-24,2	-9,3	-6,4	-3,7	-2,3	-1,4	-0,7	0,1	3,7	4,3	7,6	10,6	14,3	16,0	22,0	25,1	25,9
$R'_{\Sigma\text{ст-т}} - R'_{\Sigma\text{вода}}$	Be	Cu	U	Bi	Pb	Ga	Mg	Sc	V	Cr	Th	Fe	Al	P	K	Ba	Mn	Sr	Ce	Ca	La
	-1 430	-219	-197	-30,9	-24,1	-9,3	-6,0	-3,6	-2,3	-1,4	-0,63	3,8E-04	3,3E-03	0,28	1,1	3,6	4,1	7,5	10,6	11,7	16,0

$R'_{\Sigma\text{вода}}$	Sc	Pr	Pb	Th	Nd	La	Ce	V	Cr	Al	Fe	Ga	Sr	Ba	Mn	Rb	Ca	Zn	Ni	Tl	
	-0,11	-0,09	-0,06	-0,04	-0,03	-0,03	-0,02	-0,007	-0,006	-0,003	-3,8E-04	1,3E-03	0,05	0,08	0,22	0,42	2,61	4,53	5,10	10,2	
$R'_{\Sigma\text{ст-т}}$	Li	Rb	Yb	Ni	Pr	Dy	Gd	Sm	Er	Co	Lu	Ho	Eu	Tb	Cd	Tm	Cs	Tl			
	39,5	52,0	78,3	78,8	86,7	106	123	125	142	279	480	487	523	640	717	746	832	14 161			
$R'_{\Sigma\text{ст-т}} - R'_{\Sigma\text{вода}}$	Zn	Nd	Y	Li	Rb	Ni	Yb	Pr	Dy	Gd	Sm	Er	Co	Lu	Ho	Eu	Tb	Cd	Tm	Cs	Tl
	17,4	25,9	26,9	39,8	51,5	73,7	78,5	86,7	106	123	125	142	281	481	488	523	641	718	748	835	14 150

Table 2. Rows of differential mobility elements for filtration at pH 3 through ferruginous laterites base surface (range 6-7 meters deep wells).

$R'_{\Sigma\text{вода}}$	Tl	Cs	Tm	Tb	Lu	Eu	Ho	Cd	Rb	Er	Sm	Dy	Yb	Gd	Pr	Li	Co	U
	-50,01	-11,23	-4,33	-3,46	-3,35	-2,95	-2,63	-2,37	-1,74	-0,70	-0,68	-0,51	-0,51	-0,50	-0,42	-0,40	-0,16	-0,16
$R'_{\Sigma\text{ст-т}}$	Tl	Cs	Tm	Lu	Tb	Ho	Eu	Cd	Er	Rb	Yb	Sm	Bi	Dy	Pr	Gd	U	Li
	-17 098	-3 253	-2 624	-2 192	-1 419	-1 281	-1 162	-561	-352	-324	-317	-278	-258	-225	-178	-154	-140	-70,0
$R'_{\Sigma\text{ст-т}} - R'_{\Sigma\text{вода}}$	Tl	Cs	Tm	Lu	Tb	Ho	Eu	Cd	Er	Rb	Yb	Sm	Bi	Dy	Pr	Gd	U	Li
	-17 048	-3 242	-2 620	-2 188	-1 416	-1 278	-1 159	-558	-352	-322	-316	-277	-257	-224	-177	-154	-140	-69,6

$R'_{\Sigma\text{вода}}$	Bi	Mg	Sr	Nd	La	Cu	Y	Ce	Ga	Th	V	Cr	Mn	P	Sc	Pb	Ni		
	-0,15	-0,11	-0,11	-0,10	-0,07	-0,05	-0,03	-4,1E-03	-2,3E-03	-8,7E-04	-2,9E-04	1,5E-03	6,4E-03	7,1E-03	1,2E-02	0,14	0,19		
$R'_{\Sigma\text{ст-т}}$	Y	Nd	La	Co	Sr	Pb	Th	Sc	Ce	Cu	Zn	Ga	Mn	Cr	V	P	Fe	Mg	Ni
	-53,7	-50,5	-38,3	-37,5	-30,6	-21,0	-20,5	-16,4	-11,6	-7,1	-2,9	-2,6	-0,49	-0,47	-0,29	-0,29	0,01	0,92	377
$R'_{\Sigma\text{ст-т}} - R'_{\Sigma\text{вода}}$	Y	Nd	La	Co	Sr	Pb	Th	Sc	Ce	Cu	Zn	Ga	Mn	Cr	P	V	Fe	Mg	Ni
	-53,6	-50,4	-38,2	-37,4	-30,5	-21,2	-20,5	-16,4	-11,6	-7,0	-2,9	-2,5	-0,49	-0,47	-0,29	-0,29	0,01	1,03	377

The increase in acidity of given solutions in all cases intensifies processes of redeposition and an ionic exchange metal - proton. Experimental data will be coordinated with results of mineral structure determination and the content of trace elements in bauxites and accompanying rocks on a cross section of lateritic airing crusts.

The work was supported by the RFBR Projects No. 12-05-00509 and 11-05-00638.

References:

1. Alekhin Yu.V. (2000). Experimental methods in the theory and practice of creating geochemical barriers. *Abstracts of conference "The School of Environmental Geology and rational mining"*. St-Petersburg. pp.22-24. (in russian)
2. Alekhin Yu.V., S.M. Ilina, S.A. Lapitsky, O.S. Pokrovsky (2011). Experience a comparative analysis of the individual components of runoff of small rivers of the northern region and central Russia. *Bulletin MOIP. Section Geology:* M., MSU, , v. 86, No.1, pp. 59-81. (in russian)
3. Alekhin Yu.V., S.M. Ilina, S.A. Lapitsky, O.S. Pokrovsky, J. Viers, O.Yu. Drozdova (2012). Behavior features of rare earth elements in river flow boreal climate zone. *Bulletin MOIP. Section Geology:* M., MSU, v.87, No.5, ppc.33-42. (in russian)
4. Drozdova O.Yu., Alekhin Yu.V., S.M. Ilina, S.A. Lapitsky, M.N. Sokolova (2011). Results of research of migration mobility of microelements in the soil horizons under the influence of humic and carbonic acids. *Vestn. Otd. naukZemle, 3,* NZ6026, doi:10.2205/2011NZ000156.
5. Ilina S.M., Yu.V. Alekhin, S.A. Lapitsky, M.N. Sokolova (2011). Chromatographic separation regularities of rare earth elements on the dynamic membrane during their formation in ultrafiltration process. *Vestn. Otd. nauk Zemle, 3,* NZ6030, doi:10.2205/2011NZ000160.
6. Mamedov V.I., V.A. Bronevoi, I.O. Makstenek, V.A. Ivanov, V.V. Pokrovsky (1983). Mode of ground waters as the major supervising factor of mineralogo-geochemical ash value of airing crusts on the Liberian board. *Lithology and minerals*, No1, p. 3-11. (in russian)
7. Mamedov V.I., S.A. Vorobyev (2009). Lateritic Sheet Air. *Geochemica et Cosmochemica Acta.* Goldschmidt Conference Abstracts. P.A824.
8. Mamedov V.I., Y.V. Boufeev, Y.A. Nikitine (2010). Geologie de la republigue de Guinee. *Min. des Mines et de la Geologie de la Rep. De Guinee; GEOPROSPECTS* Ltd; Univ. d'Etat de Moscou Lomonossov (Fac. Geol.) Conakry – Moscou: Aquarel,. 320 p.

Bublikova T.M., Balitsky V.S., Setkova T.V. Study of basic copper carbonate solubility in aqueous ammonia solutions (theoretical and experimental data)

Institute of Experimental Mineralogy RAS, Chernogolovka

Abstract. The solubility of basic copper carbonate was studied theoretically and experimentally in 1.0, 2.0, 3.0*m* ammonia solutions at temperature range of 25-80°C and pressure of 0.1 MPa. The phase diagrams of solubility of $CuO-CO_2-H_2O-NH_3$ system were plotted and defined stability fields of basic copper carbonates depending on the CO_2 pressure and the ammonia concentration.

Key words: malachite, azurite, solubility, thermodynamic calculation.

Citation: Bublikova T.M., V.S. Balitsky, T.V.Setkova (2013). The study of the basic copper carbonate solubility in aqueous ammonia solutions (theoretical and experimental data).

Experimental and theoretical investigations of malachite solubility was carried out as a part of search of copper carbonates (malachite and azurite) crystallization conditions. We have demonstrated previously, that the most promising for the malachite and azurite synthesis are the water-ammonia solutions. The malachite have a high solubility is those solutions [Balitsky & Bublikova, 1990]. Experimentally a solubility of $CuCO_3{\bullet}Cu(OH)_2$ has been studied in 1, 2, 3m aqueous ammonia solutions at 25 50, 75°C. An initial material was placed in ampoules made of thermal-resistant glass, then it was grouted of ammonia solution of necessary concentration. The ampoules were sealed and placed into thermostat. After equilibration, the ampoules were unsealed, and an aliquot part of the solution was filtered and analysed for a total copper content. To speed up the process of dissolving the contents periodically (4-12 hours) is mechanically mixed. Equilibrium was considered to be achieved when the concentration of copper in the solution did not change. The most intensive dissolution of the basic copper carbonate in all cases occurred in the first 6 - 10 hours. We used the volumetric iodometric method for estimation of the copper content and a total CO_2 content in solution was determined using AN-7529 express-analyzer. The absolute error of the method was ± 0.2 mg / ml.

Phase relations in the system $CuO-CO_2-H_2O-NH_3$ were studied by calculating and plotting of diagrams of copper solubility for temperatures 25 to 80°C, pressure 0.1 MPa using a HCh software package [Shvarov & Bastrakov, 1999]. Thermodynamic properties of the substances used in the calculation were determined using published data and previously obtained by us [Bublikova, 1989]. Analysis of phase equilibria was carried out on sections of the space compositions of the system at constant mole concentration of ammonia 0, 1.0, 2.0 and 3.0m (Fig. 1a, b, c).

Experimental results are presented in Table 1 and Figure 1. They show that the equilibrium copper content increases with ammonia concentration increasing and decreases with temperature rise in ammonia solutions. It can be seen that the temperature dependence is manifested in a sharper, higher than the initial concentration of the water-ammonia solutions.

Malachite is unstable in the ammonia solution at given condition it decomposes with tenorite forming that was confirmed by the thermodynamic calculations. Malachite solubility have retrograded character in this case.

The results of theoretical calculations and our experimental data on the solubility of basic copper carbonate (Fig.1d) are in good agreement with Wang et al [Wang, 2009] results on malachite solubility in ammonium chloride solutions.

Studies were the basis for developing a method of synthesis of jewelry and semi-precious malachite and may be important in the development of hydrometallurgical methods for obtaining copper from poor native and oxidized ores, including those from the old dumps and abandoned underground mines. These methods are based on the selective dissolution of copper minerals in ammonia solutions also.

This work was supported by Ministry of education and science of Russian Federation (Agreement no. 8612). Authors thank A.F. Redkin for consultation on thermodynamic calculations.

Table 1. Results of determination of copper content at dissolution of basic copper carbonate in aqueous ammonia solutions

№	Concentration of solution, NH_3	Temperature,°C	Cu concentration in equilibrium solution, mg/ml
1	1.0	25	12.37±0.15
2	2.0	25	31.15±1.14
3	3.0	25	47.07±1.80
4	1.0	50	12.20±0.52
5	2.0	50	28.42±1.40
6	3.0	50	40.30±1.72
7	1.0	75	11.26±0.78
8	2.0	75	27.98±1.93
9	3.0	75	32.18±1.80
10	2.0	25	30.75±1.44
11	2.0	75	27.98±1.35

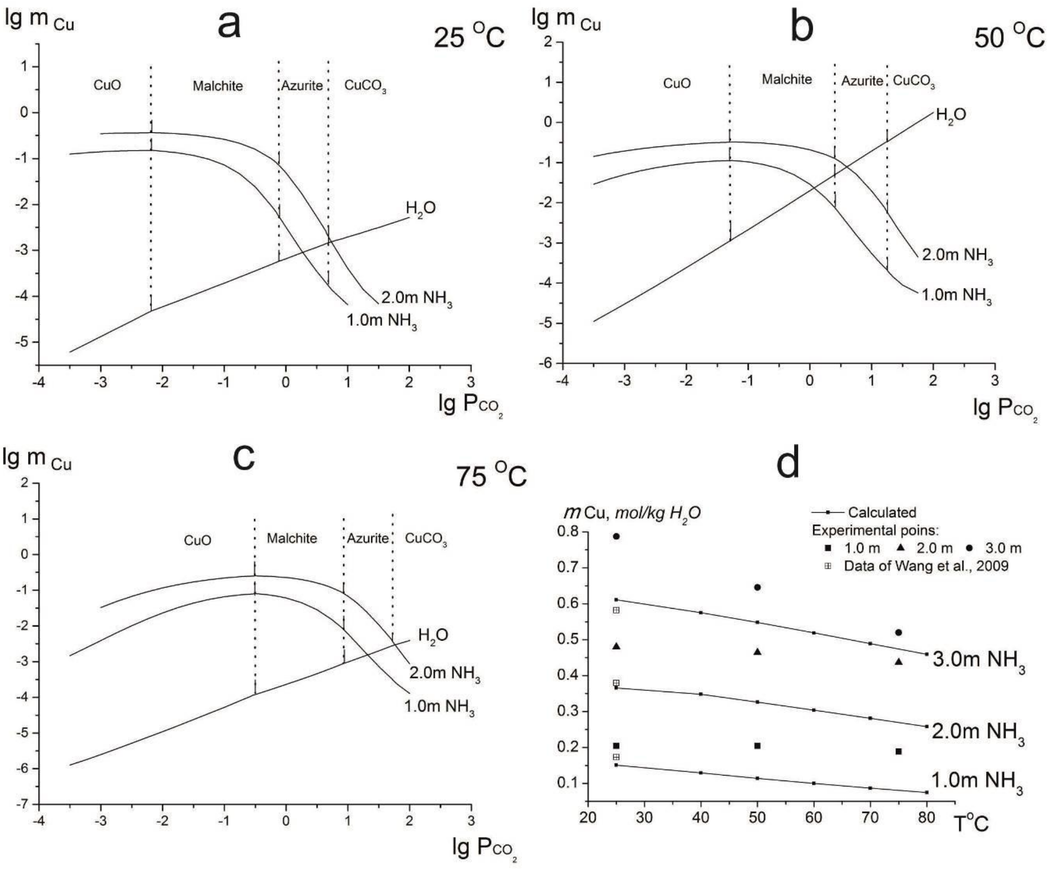

Fig. 1 a,b,c. – isothermal diagrams of solubility CuO-CO_2-H_2O-NH_3 system at pressure of 0.1 MPa;   - calculated and experimental data of malachite solubility as functions of NH_3 concentration and temperature.

References:

1. Balitsky V.S., T.M. Bublikova (1990). Phisico-chemical foundations of malachite synthesis and structural-morphological peculiarities and properties of its man-made jewelry quality varieties. *Prog. Crystal Growth and Charact*., 21, 139-161.
2. Bublikova T.M., V.A. Pokrovsky, V.S. Balitsky, A.F.Gurov (1989). Thermodynamic function of natural and synthetic malachite at high temperatures. *Abst. II All-Union Gemmology conf.*, Chernogolovka, 183.
3. Shvarov Yu. V., E.N. Bastrakov (1999). HCh: a software package for geochemical equilibrium modelling. *User's Guide. — AGSO Record* 1999/25, Canberra.
4. Wang Xi et al. (2009). Solubility prediction of malachite in aqueous ammoniacal ammonium chloride solutions at 25°C. *Hydrometallurgy,* 99, 231-237.

Dadze T.P., Kashirtseva G.A., Novikov M.P., Plyasunov A.V. Experimental study of the solubility of Moo$_3$ in water under hydrothermal conditions

Institute of Experimental Mineralogy RAS, Chernogolovka

Abstract. The solubility of MoO_3 in water is experimentally determined at various temperatures and pressures. It is shown that the solubility of MoO_3 increases with increasing temperature from 200°C to 400°C at a constant pressure of 500 bar. In experiments at T=300°C, the solubility increases when the pressure grows from 100 bar to 500 bar, and remains virtually unchanged at higher pressures up to 1000 bar. The experimental determined high solubility's of molybdenum oxide under hydrothermal parameters explain its rare finding in nature.

Key words: Experiment, molybdenum trioxide, solubility, hydrothermal parameters.

Citation: Dadze T.P., G.A. Kashirtseva, M.P. Novikov, A.V. Plyasunov (2013). Experimental study of the solubility of Moo$_3$ in water under hydrothermal conditions. Vestnik Otdeleniya nauk o Zemle

The goal of this study was to investigate the effect of temperature and pressure on the solubility of MoO_3 in water at hydrothermal conditions. The crystalline molybdenum trioxide for the solubility experiments was obtained by calcination of ammonium molybdate of the reagent grade purity [Koryakin and Angelov, 1974]. Experimental runs were conducted in titanium autoclaves made from the alloy VT-8, passivated with 20% nitric acid at 400°C for one day. The pressure in the autoclave was calculated from the filling coefficient using the PVT-data for water. A precisely weighed amount of crystalline MoO_3 was placed in a titanium container, suspended on the obturator at the top of the autoclave. Autoclaves were quenched under running cold water for 5-7 minutes. The time to reach equilibrium was taken in accordance with the literature data [Ivanova et al., 1975]. The composition of solid phases before and after the experiments was determined by X-ray analysis, which showed that after the experiments the solid phase was only crystalline MoO_3. In all experiments, a twice-distilled water was used. The concentration of molybdenum in solution after the experiment was determined by the colorimetric method on Specol-11 at λ = 453 nµ and duplicated by measurements of the weight loss. The satisfactory agreement of analytical determinations of the concentration of molybdenum in solution with the weight loss results of the container with MoO_3 (when recalculated to Mo) should be noted. The experimental data presented in Tables 1, 2 and Figures 1, 2.

Table 1. The pressure dependence of the solubility of MoO_3 in water at T=300°C

№	Code of the run	P,bar	Chemical analysis data		
			mg/ml	mol/kg H_2O	lg $m_{Mo(VI)}$
1	1	100	0.40	0.0041	-2.38
2	2	100	0.45	0.0047	-2.33
3	3	100	0.37	0.0038	-2.42
4	24	160	0.73	0.0076	-2.12
5	32	160	0.66	0.0069	-2.16
6	4	200	0.73	0.0076	-2.12
7	6	200	0.48	0.0050	-2.30
8	26	200	0.78	0.0081	-2.09
9	33	200	0.79	0.0110	-1.96
10	9	500	1.19	0.0120	-1.906
11	28	500	1.18	0.0120	-1.91
12	29	500	1.18	0.0120	-1.91
13	30	1000	1.26	0.0130	-1.88
14	31	1000	1.25	0.0130	-1.88

Table 2. Temperature dependence of the MoO_3 solubility in water at P=500 bar

№	Code of the run	T, °C	Chemical analysis data		
			mg/ml	mol/kg H_2O	lg $m_{Mo(VI)}$
1	17	200	1.18	0.012	-1.92
2	18	200	0.99	0.010	-2.0
3	9	300	1.19	0.012	-1.91
4	28	300	1.18	0.012	-1.91
5	29	300	1.18	0.012	-1.91
6	52	394.6	2.92	0.030	-1.52
7	53	394.6	2.80	0.029	-1.54
8	62	412	4.03	0.042	-1.38
9	63	412	3.85	0.040	-1.40

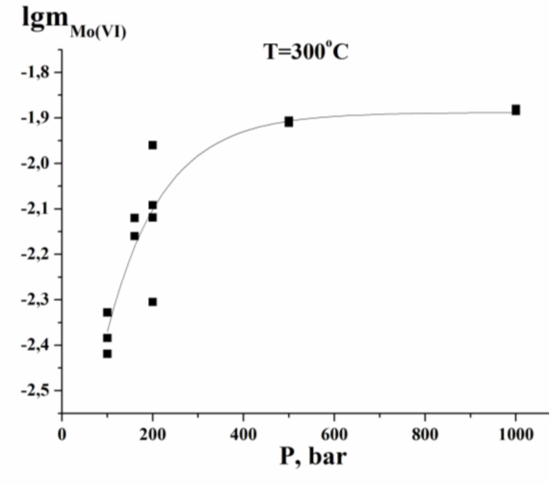

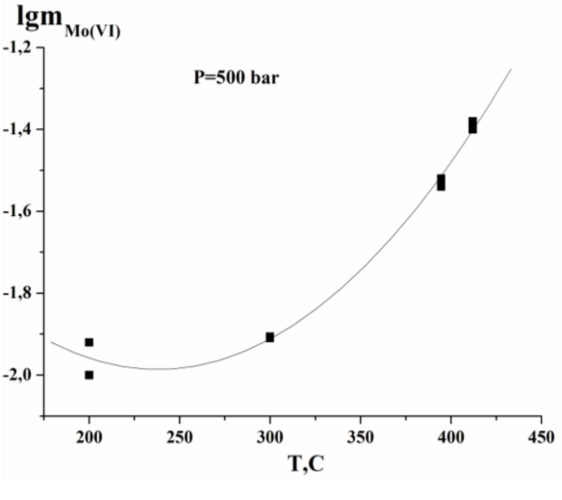

Fig. 1. Pressure dependence of the MoO_3 solubility in water
Fig. 2. Temperature dependence of the MoO_3 solubility in water at P=500 bar

The presented data show that at T=300°C, with increasing pressure from 100 bar to 500 bar the solubility of MoO_3 increases, and at higher pressures up to 1000 bar it remains virtually unchanged. At a constant pressure of 500 bar the solubility of MoO_3 increases with increase of temperature from 200°C to 400°C.

Geological observations indicate that hydrothermal deposits practically never contain MoO_3. This is probably due to the high solubility of the oxide in a wide range of temperature and pressure.

This work was supported by RFBR (grant 11-05-00786-a).

References:

1. Ivanova G.F., N.I. Levkina, L.A. Nesterova et al. (1975). Equilibria in the system MoO_3-H_2O at temperatures 25-300 °C. *Geokhimiya,* No 2, p. 234-247.
2. Koryakin Yu.V., I.I. Angelov (1974). Pure chemicals. M.: “Khimiya”, 406 pp (in Russian).

Zharikov ^{1,2}A.V., Vitovtova^{2}V.M., Lebedev^{3}E.B., Rodkin^{4}M.V. Transport properties of crystalline rocks: the results of laboratory measurements and the estimations on the basis of geological and geophysical data

[1]Institute of Geology of Ore Deposits, Petrography, Mineralogy and Geochemistry, RAS, Moscow

[2] Institute of Experimental Mineralogy RAS, Chernogolovka

[3] V. I. Vernadsky Institute of Geochemistry and Analytical Chemistry RAS, Moscow

[4]Institute of Earthquake Prediction Theory and Mathematical Geophysics, RAS, Moscow

Abstract. A correlation between results of the experimental study of transport properties of crystalline rocks carried out under *PT*-parameters corresponding to the deep horizons of the Earth's crust, geological and seismic data is presented.

Key words: permeability, experiment, high temperature and pressure, continental crust, seismicity.

Citation: Zharikov A.V., V.M. Vitovtova, E.B. Lebedev, M.V. Rodkin (2013). Transport properties of crystalline rocks: the results of laboratory measurements and the estimations on the basis of geological and geophysical data. Vestnik ONZRAN*, 5*, (doi: -)

Rock transport properties (first of all permeability and porosity) govern the fluid regime, mass and heat transfer in the lithosphere. At the present time there are no remote geophysical methods available for direct determination of deep seated rock permeability and porosity. However, permeability data at high *PT* simulating the *in situ* conditions can be obtained in the laboratory on relevant rock samples. Then with use of this data effective pore diameters and effective porosity values can be determined.

This paper presents the results of transport properties studies on the samples of tight rocks at the *PT* conditions of the deep continental crust and metamorphic transformations, as well, in comparison with geological and seismic data.

Experimental data. Permeability is strongly controlled by pressure and temperature. With pressure increase (at *T*=const) permeability decreased in all the studied samples. Temperature increase at constant pressure lead to monotonous permeability increase or decrease within the entire temperature range, or to inversions on the trends: permeability firstly decreased, reached its minimum value and then increased (Fig. 1). It is significant that the thresholds frequently occur on the permeability trends.

It was found that such permeability behavior is governed by changes in the rock microstructure (state of microfracturing) resulted of the competitive effects of temperature and pressure [Shmonov et al., 2002]. The behavior of microcracks with different aspect ratio (ratio of microcrack aperture to its length) is different under heating [Zharikov et al., 2003].Consequently, the inversions may appear on the trends. The main cause governing permeability of tight rocks is a degree of interconnection of fluid conductive clusters of microcracks. Even slow changes in microcrack density, length or aperture due to temperature or pressure effect may lead to dramatic permeability changes. So, the thresholds appear on the permeability trends.

The permeability trends for the samples of typical rocks of continental crust obtained at simultaneous temperature and pressure elevation simulating the *in situ* depth increase are presented in Fig. 2. Fig. 3 shows the dependence of porosity, which values are calculated with use of experimental data, on permeability [Vitovtova et al., 2011] Pressure effect prevails and, as a result, permeability and porosity decrease with depth increase for all the studied samples.

In contrast, heating up to 500 - 600°C that corresponds to conditions of progressive metamorphism usually leads to permeability increase (Fig. 1 c, d). In case of water occurrence such tendency intensifies Fig. 4 [Zharikov et al., 1993].

Petrological data. From the petrological data both the marks of long periods of very low permeability and quite short events of high permeability may be found in the rock samples. Fluid intrusions occupying, as a rule, isolated positions in the corners of mineral grains indicate rather low values of rock paleopermeability. Nevertheless, linear and planar structures with high density of such inclusions, which probably served as interconnected channels for fluids in the past, were found (Fig. 5) [Fusseis & Handy, 2008].

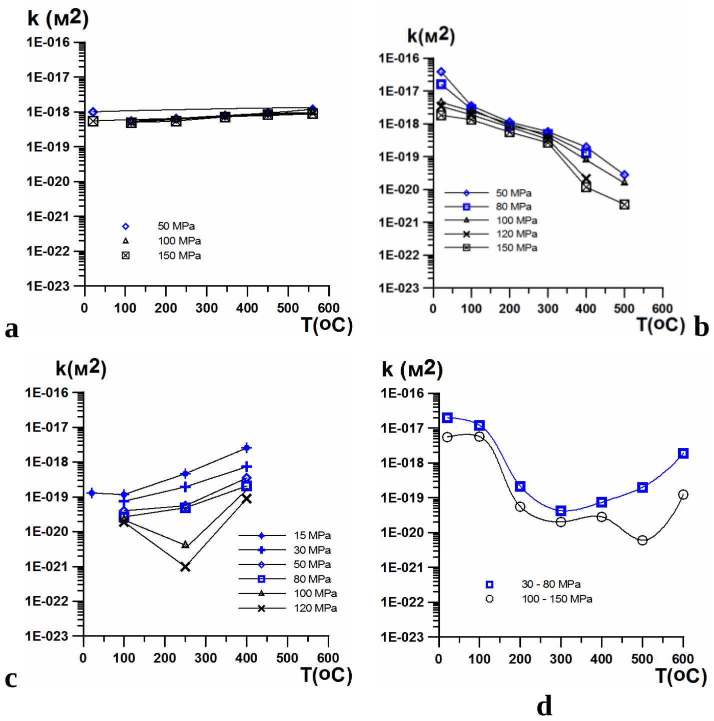

Fig. 1. Permeability vs temperature, P_{eff}=const.
a – marble, sam. 1, b – granodiorite, sam. 82066, c –granite, sam. 2., d - amphibolite, sam. 43639.

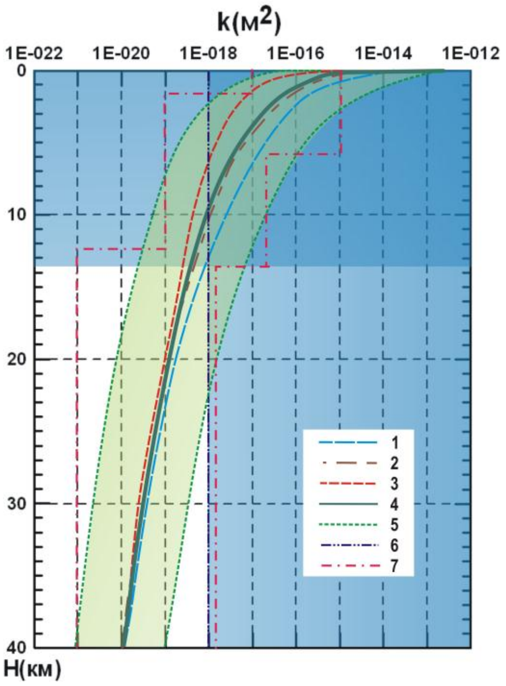

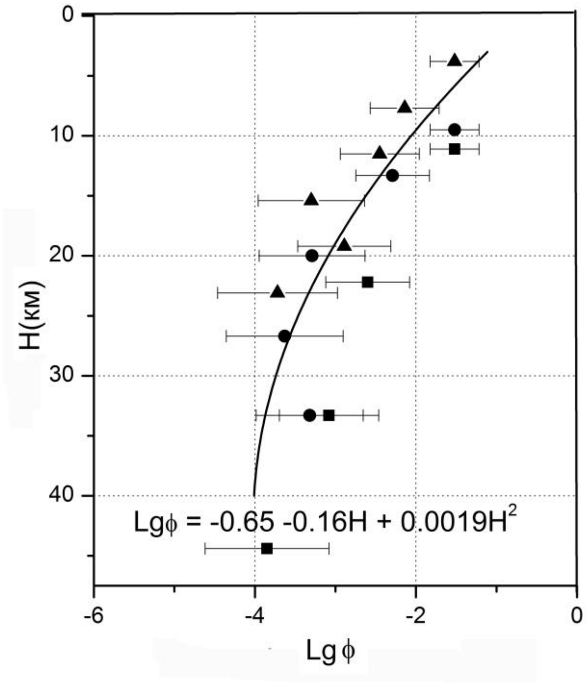

Fig. 2. The permeability dependencies obtained with simultaneous increase of temperature and pressure simulating *in situ* conditions of continental crust: 1- trend for temperature gradient of 9°C/км, 2- trend for temperature gradient of 15°C/км, 3- trend for temperature gradient of 26°C/км, 4- generalized trend, 5- limits of 90 % confidence interval, 6- 10^{-18} m^2 – according to D. Norton (1979) minimal permeability value when hydrothermal systems can operate, 7- permeability according geophysical data.

Fig. 3. The dependence of continental crust rocks porosity on depth developed on the basis of the experimental data on permeability.

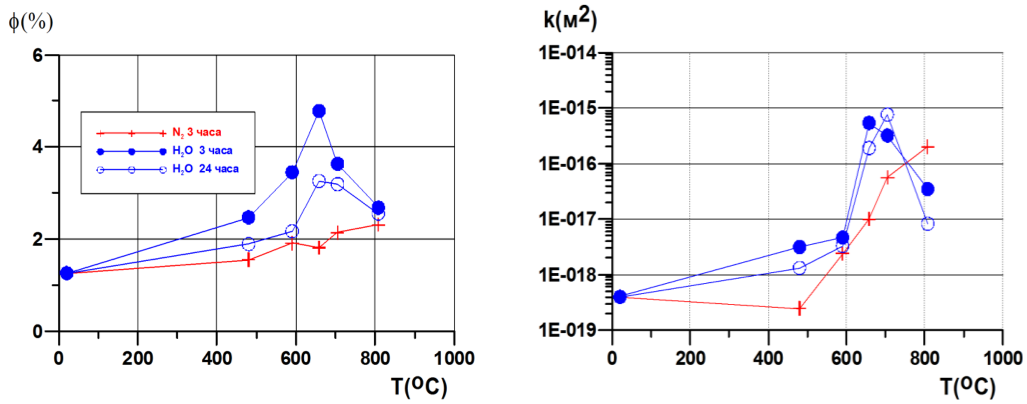

Fig. 4. Dependencies of porosity (a) and permeability (b) of amphibolite heated under gas pressure in dry conditions and under water pressure $P_{conf}=P_{fl}$=300 MPa on quenching temperature.

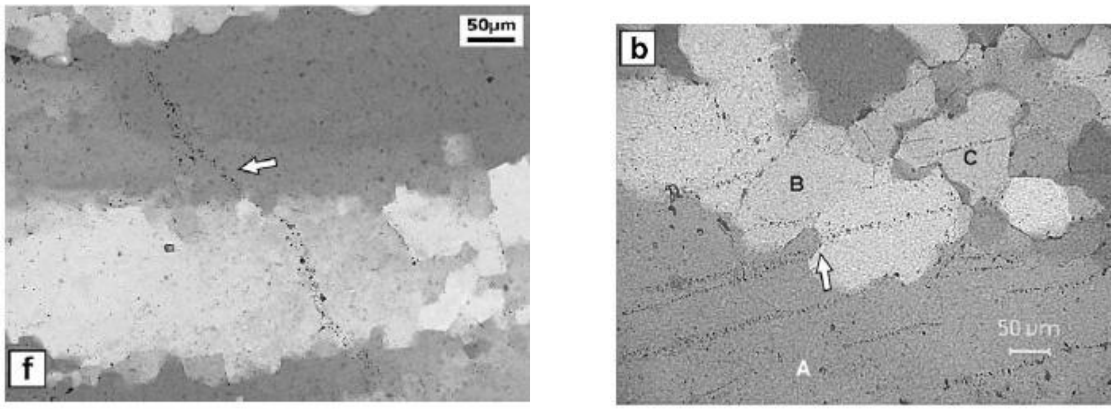

Fig. 5. Linear and planar structures with high density of fluid inclusions, which probably indicate paleo fluid permeable channels [Fusseis & Handy, 2008].

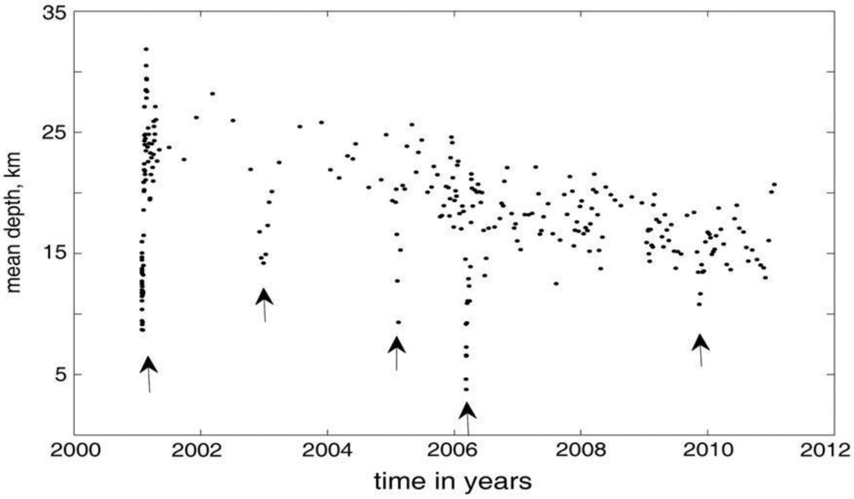

Fig. 6. Mean values of depth for groups of 20 consecutive events in the 2001 Bhuj earthquake sequence with time expired from the Bhuj mainshock occurrence.

Seismic data. In the seismic regime the periods of extraordinary high seismic activity with unusual properties presumably associated with the fluid activity can be found. The example of the aftershock sequence of Bhuj earthquake examined in details (Mw7.7, 2001, Kachchh area, India) is presented in Fig. 6. Besides the anomalies of b-value and mean depths, increase of apparent stresses in the seats and decrease of fractal (correlative) dimensions of their hypocenters are typical for the "bursts" of seismicity. We suppose that such bursts of seismic activity are related to ejection of the deep fluids to the Earth's surface. The effective background permeability of the mid-crust in the region of Bhuj 2001 earthquake was evaluated according to the tendency of aftershock shifting (emersion) with depth and was estimated according to [Miller et al., 2004] to be about $k \approx 10^{-13}$ m^2.

Conclusions. The results of the experiments show that the values of rock permeability can change by decimal orders due to the effect of high temperature and pressure. In general it was found that permeability of the continental crust rocks decreases with depth [Shmonov et al., 2002]. In contrast, its increases at *PT*-parameters of progressive metamorphic transformations [Shmonov et al., 2002; Zharikov et al., 1993].

The results of petrologic studies reveal both the marks of long periods of very low permeability and events of high permeability.

The conception when long periods of low permeability are coupled with short periods of high permeability is supported by seismic data. The burst of hypocenters clouds to the Earth surface and/or their systematical movement up to the Earth surface are found using the data of the earthquakes localization. Identification of such events with front of fluid propagation allows to estimate according to [Miller et al., 2004] high permeability values as ($\approx 10^{-13}$ m^2).

However, the mechanism of increase of permeability of mid-crust is unclear. Moreover, we suggest that some episodes of the crust permeability increase could be related to the positive feedbacks, between microcrack initiation due to rock metamorphic transformations resulting in increase of permeability and active deep fluid infiltration which in its turn accelerates the rate of metamorphic transformations. The experimental data [Zharikov et al., 1993] prove this suggestion.

The work is supported by RFBR (grant # 11-05-00778) and by RAS (Programs 4 and 9).

References:

1. Fusseis F, M.R. Handy (2008). Micromechanisms of shear zone propagation at the brittle–viscous transition. *Journal of Structural Geology*, V. 30, pp. 1242–1253.
2. Miller S.A., C. Collettini, L. Chiaraluce et al. (2004). Aftershocks driven by a high pressure CO_2 source at depth. *Nature*, V. 427, pp. 724-727.
3. Shmonov V.M., V.M. Vitovtova, A.V. Zharikov (2002). *Fluidnaja pronizaemost porod zemnoy cori* (Fluid permeability of the rocks from the Earth crust), Nauchniy Mir, Moscow.
4. Vitovtova1 V.M., V.M. Shmonov, A.V. Zharikov (2011). Distribution of the pore sizes in the continental crust: inferences from experimental data about Permeability. *Vestnik Otdelenia nauk o Zemle RAN*, V. 3, NZ6018, doi:10.2205/2011NZ000148
5. Zharikov A.V., A.A. Pek, E.B. Lebedev, A.M. Dorfman, S.R. Zebrin (1993). The effect of water fluid at temperature up to 850°C and pressure of 300 MPa on porosity and permeability of amphibolite. *Physics of the Earth and Planetary Interiors*, V. 76, No 3/4, pp. 219-227.
6. Zharikov A.V., V.M. Vitovtova, V.M. Shmonov, A.A. Grafchikov (2003). Permeability of the rocks from the Kola superdeep borehole at high temperature and pressure: implication to fluid dynamics in the continental crust. *Tectonophysics*, V. 370, No. 1-4, pp. 177-191.

Korzhinskaya V.S. The influence of chloride concentration on pyrochlore solubility at T= 550°C, P = 1000 bar

Institute of Experimental Mineralogy RAS, Chernogolovka

Abstract. Experimental results of the behavior of natural pyrochlore are presented in chloride solutions of HCl, KCl, and NaCl with concentrations from 0.01 to 2 m at T = 550°C, P = 1000 bar in the presence of oxygen buffer Co-CoO. It was found that the pyrochlore dissolves incongruently. In HCl solutions, niobium content slightly increases with increasing HCl concentration and is within $n*10^{-4}$- $n*10^{-3}$ mol/kg H_2O. In KCl and NaCl solutions, equilibrium niobium content is much lower ($n*10^{-7}$-$n*10^{-6}$ mol/kg H_2O). For sodium and calcium, it is observed a significant positive correlation of the chlorides concentration, especially in NaCl solutions, where it reaches values of 0.1-0.395 mol/kg H_2O.

Key words: experiment, pyrochlore, solubility, buffer, chloride.

Citation: Korzhinskaya V.S. (2013). The influence of chloride concentration on pyrochlore solubility at T = 550°C, P = 1000 bar. *Vestn.Otd. nauk Zemle,* (doi:

We carry out a systematic experimental study on solubility of stable under natural conditions of the mineral phase tantalum niobate of complex composition (columbite, pyrochlore, etc.). For natural pyrochlore (Ca, Na)$_2$ (Nb, Ta)$_2$O$_6$ (O, OH, F) were previously conducted experimental studies on its solubility in solutions of HF and KF [Korzhinskaya, 2011]. We continued experimental studies on the pyrochlore solubility in chloride solutions.

The experimental results of the effect of chloride solutions (HCl, KCl, and NaCl) on the niobium, calcium and sodium solubility at T = 550° C, P = 1000 bar under Co-CoO oxidizing conditions are presented. For the experiments a monocrystal of pyrochlore was selected from weathering crust of carbonatite located in the Tatarka deposit. Its composition, estimated by microprobe Cam Scan in wt % is Na_2O -7.61; CaO -14.28; Nb_2O_5-71.61; F-5.18; TiO_2 - 0.83; $Ta_2O_5 \leq 1$. The concentration of HCl, KCl, and NaCl solutions ranged from 0.01 up to 2m. The run duration was 15 days. Experiments were performed in platinum capsules (10x0.2x60 mm) on hydrothermal high pressure apparatuses. The quenched solution was analyzed by ICP/MS and ICP/AES methods (mass spectrometry and atomic emission) for Nb, Ta, Mn, and Fe and admixture elements Ti, W, and Sn. To determine the chemical composition of the newly formed phases the solid run products were studied using X-ray microprobe (Cam Scan MV2300 (VE GA TS5130MM) methods of analysis.

The concentration dependence of niobium content in HCl, KCl, and NaCl solutions is shown in Fig. 1. As can be seen from the figure, the niobium content slightly increases from $2.75*10^{-4}$ to $2.63*10^{-3}$ m as the HCl concentration increases from 0.01 to 2 m. In the initial solutions of KCl and NaCl the concentration curves practically coincide. In 0.01m solutions KCl and NaCl solutions the Nb content is, respectively, $1.40*10^{-7}$ and $1.70*10^{-7}$ m. With increasing KCl and NaCl concentrations to 2 m, the niobium content increases by an order and achieves values of $2.19*10^{-6}$ in 2 m KCl and $2.95*10^{-6}$ mol/ kg H_2O in 2 m NaCl. The comparing graph of the niobium content at the pyrochlore solubility in HF and HCl solutions is shown in Fig. 2. As can be seen from the figure, at the acids concentration 0.01m-0.1m, the Nb content is higher in HCl. In 0.01m HCl solution it is by 2.5 orders of magnitude higher. In 0.1m HCl the Nb content is comparable with the niobium content in 0.1m HF. With increasing acids concentrations the niobium content is by 2-2.5 orders of magnitude higher in HF solution. In 1 and 2m HCl and NaCl solutions pyrochlore dissolves incongruently. In this case, the new phases $Ca_2Nb_2O_6F$ and $NaNbO_3$ are formed.

Experimental data on the pyrochlore solubility as a function of the total concentration of KF and KCl are shown in Fig. 3. The data show that at all KF concentrations the Nb content is s higher in KCl solutions. At low concentrations it is by 1-1.5 orders of magnitude higher. At 1and 2m concentrations the Nb content is by 2.5 orders of magnitude higher. Fig. 4 and 5 shows the concentration dependence of the contents of Na and Ca in the chloride solution (HCl, KCl, and NaCl). The Ca concentration strongly increases with increasing HCl concentration and achieves values $n*10^{-5}$ mol/kg H_2O in 0.01m HCl and $n*10^{-2}$ mol/kg H_2O in 2m HCl (Fig. 5). In KCl and NaCl solutions the calcium content does not change with increasing chloride concentrations. In all chloride solutions the Na content also increases with increasing chloride concentration. The highest Na contents are detected in NaCl and HCl solutions. In KCl solutions the Na content is by of 3 orders of magnitude lower.

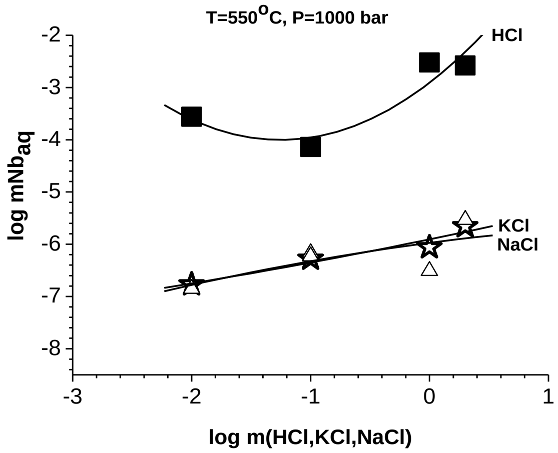

Fig. 1 Concentration dependence of niobium content at pyrochlore solubility in HCl, KCl, NaCl solutions (T = 550°C, P = 1000 bar, Co-CoO buffer)

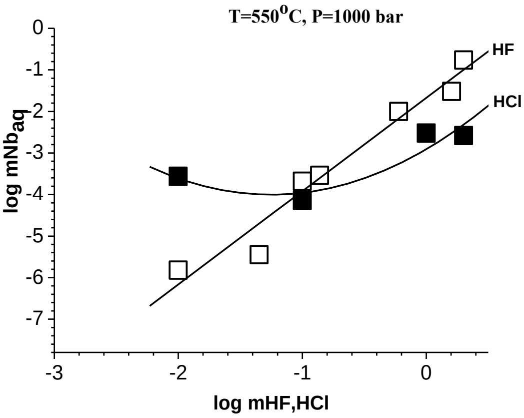

Fig. 2 Concentration dependence of niobium content at pyrochlore solubility in HF and HCl solutions (T = 550°C, P = 1000 bar, Co-CoO buffer)

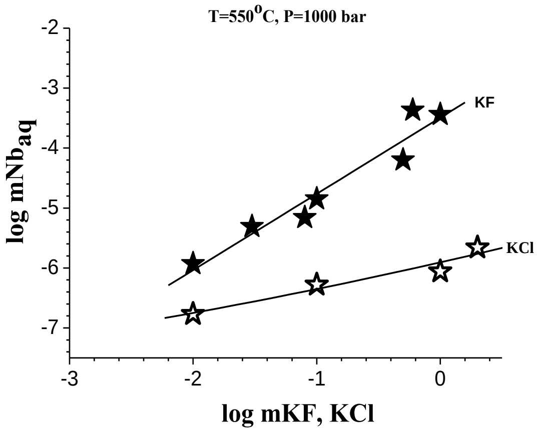

Fig. 3 Concentration dependence of niobium content at pyrochlore solubility in KF, and KCl solutions (T = 550°C, P = 1000 bar, Co-CoO buffer)

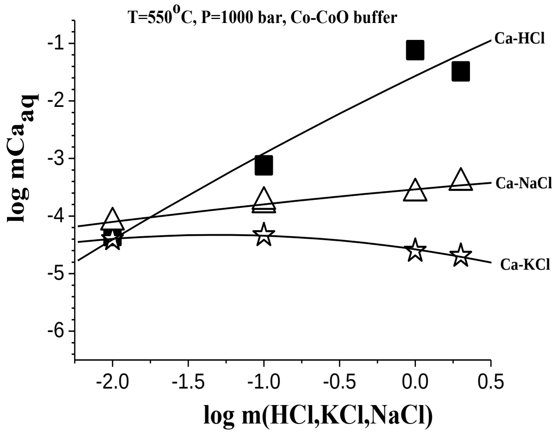

Fig. 4 Concentration dependence of calcium content at pyrochlore solubility in HCl, KCl, NaCl solutions (T = 550°C, P = 1000 bar, Co-CoO buffer)

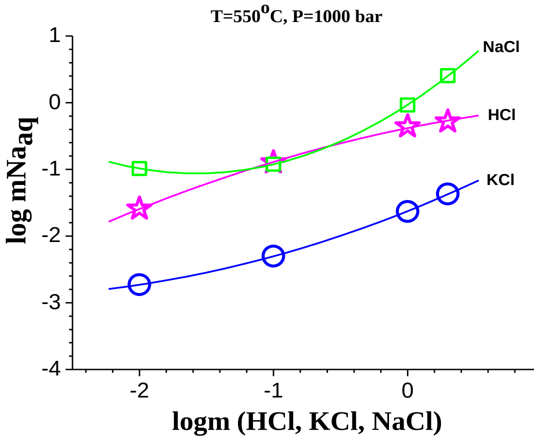

Fig. 5 Concentration dependence of sodium content at pyrochlore solubility in HCl, KCl, NaCl solutions (T = 550°C, P = 1000 bar, Co-CoO buffer)

The results obtained clearly show incongruent dissolution of pyrochlore in chloride solutions with advantageous transition in a solution of sodium and calcium compared to niobium. On this basis one can conclude that in chloride solutions the solubility product of pyrochlore is achieved due to the high sodium and calcium concentration in the solution at the lower solubility of niobium.

Acknowledgements: The work was done with the financial support of the ONZ-2 Program.

Reference

1. Korzhinskaya, V.S., (2011). Experimental study of dependence of pyrochlore solubility in HF and KF solution at T= 400°,550°C and P = 1000 bar. Vestn. Otd. nauk Zemle 3, NZ6042, doi:10.2205/2011NZ000172.

Korzhinskaya V.S., Kotova N.P. Comparative analysis of tantalite and Ta oxide solubility in the chloride aqueous solutions at T = 550°C, P = 1000 bar (Co-CoO buffer)

Institute of Experimental Mineralogy RAS, Chernogolovka

Abstract. The dependence of Mn-tantalite and Ta_2O_5 solubility as a function of chloride concentration was investigated in HCl, KCl, NaCl, and LiCl solutions with concentrations from 0.01 to 2 m at 550°C and 1000 bar under Co-CoO oxidizing conditions. The experimental data show that concentration of Ta in equilibrium with Mn-tantalite and tantalum oxide is low (near $10^{-7.5}$ - $10^{-5.5}$ m) in all chloride solutions. This is due to the fact that in all chloride solutions, Mn- tantalite dissolves incongruently. The Mn concentration in the solution is 3 to 5 orders of magnitude higher than the Ta one. Comparison of the results for Mn-tantalite and Ta_2O_5 confirms the thesis that the solubility of simple oxides (Ta_2O_5 and Nb_2O_5) restricts the upper limit of these elements concentration in hydrothermal solutions.

Key words: experiment, pyrochlore, solubility, buffer, chloride.

Citation: Korzhinskaya V.S., N.P. Kotova (2013). Comparative analysis of tantalite and Ta oxide solubility in the chloride aqueous solutions at T=550°C, P=1000 bar (Co-CoO buffer) *Vestn.Otd. nauk Zemle,* (doi:

Concentration dependence of synthetic Mn-tantalite and tantalum oxide solubility was experimentally determined in HCl, KCl, NaCl and LiCl solutions with concentrations from 0.01 to 2 m at 550°C and 1000 bar under Co-CoO oxidizing conditions.

For these purposes the pure Mn-tantalite ($MnTa_2O_6$) was synthesized from mixture of MnO (high grade) and Ta_2O_5 (pure grade) at T = 500°C, P = 1000 bar. Tantalum pentoxide has been preliminary purified by recrystallization in 0.01m HF at 500°C and P = 1000 bar. The Mn-tantalite synthesis was carried out on a hydrothermal apparatus of Tuttle type in the sealed platinum capsules (80 mm long, 6 mm diameter, 0.2 mm wall thickness). A charge of 200 mg of oxides stoichiometric mixture was placed into the Pt capsule with 0.01m HF solution. The synthesized product was analyzed using X-ray diffraction and electron microprobe analysis (Cam Scan MV2300 (VE GA TS5130MM). The crystals obtained are plate- prismatic habitus. The crystal size was 10 by 30 microns.

Experiments on the solubility of $MnTa_2O_6$ and Ta_2O_5 were carried out in welded platinum capsules at hydrothermal installation of high pressure. The run duration was 15 days. The quenched aqueous solutions were analyzed by ICP/MS (Inductively Coupled Plasma Mass Spectrometry) and ICP/AES (Atomic Emission Spectroscopy) procedures. Solid run products were studied by X-ray phase and micro-probe analysis method.

The dependence of Mn-tantalite and Ta_2O_5 solubility as a function of chloride concentration was investigated in HCl, KCl, NaCl, and LiCl solutions. In chloride solutions, Mn- tantalite dissolves incongruently. In HCl, KCl, and LiCl solutions, Ta_2O_5 dissolves congruently. The exception is the data on Ta_2O_5 solubility in NaCl solutions in which tantalum oxide dissolves incongruently.

Experimental data on the solubility of Mn-tantalite and Ta_2O_5 as a function of the total concentrations of HCl, KCl, NaCl, and LiCl are shown in Fig. 1-4. It is established that the tantalum content for the mineral and Ta oxide is lower by several orders of magnitude than that in fluoride system [Zaraisky, Korzhinskaya, Kotova, 2010]. At the same time, in HCl, KCl, and LiCl solutions the Ta_2O_5 solubility is higher by 1-2 orders of magnitude than the Mn-tantalite one. However, in NaCl solutions with concentrations from 0.01 to 0.1 m the content of Ta for Mn-tantalite is the order of magnitude less than that for Ta_2O_5. At high NaCl concentrations (1-2 m) the content of Ta for Mn-tantalite is 0.5 order of magnitude less than that the Ta_2O_5 one. This can be explained by incongruent dissolution of tantalum oxide in NaCl solutions. In this case perfectly faced crystals of natrotantite ($Na_2Ta_4O_{11}$) with classical hexahedral structure of pyrochlore are formed as a solid phase.

Concentration dependence of the Mn content on the solubility of $MnTa_2O_6$ in chloride solutions (HCl, KCl, NaCl и LiCl) is shown in Fig. 5.

The highest Mn concentrations (10^{-2} and 10^{-1} m) were detected in 0.1 and 1 m HCl solutions. In these solutions, the concentrations of Mn are, respectively, 1.5 and 2 orders of magnitude more than those in HF solutions. In all other chloride solutions concentration of manganese is also much higher than in fluoride solutions. The experimental results clearly show sharply incongruent solubility of $MnTa_2O_6$ in chloride solutions with a predominant transition to the solution of manganese compared to tantalum. The study of solids run products on a microprobe detects the presence of various the newly formed phases in HCl, KCl and LiCl solutions

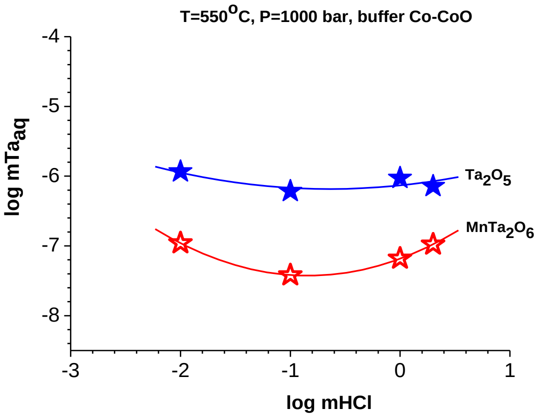

Fig.1. The solubility of Mn-tantalite and Ta_2O_5 as a function of HCl concentration at T = 550°C, P= 1 kbar (Co-CoO buffer)

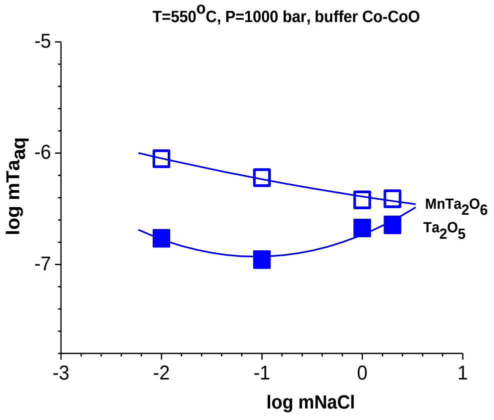

Fig.2. The solubility of Mn-tantalite and Ta_2O_5 as a function of NaCl concentration at T = 550°C, P= 1 kbar (Co-CoO buffer)

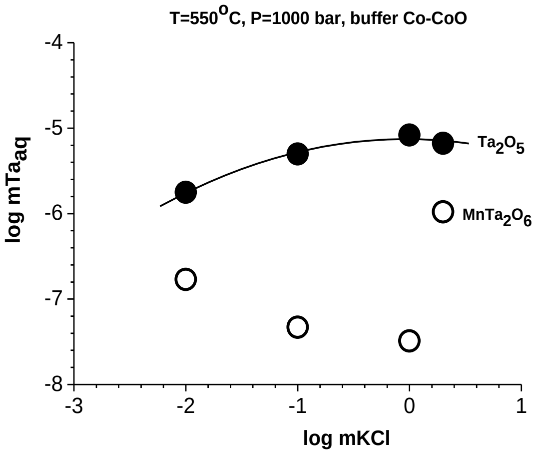

Fig.3. The solubility of Mn-tantalite and Ta_2O_5 as a function of KCl concentration at T = 550°C, P= 1 kbar (Co-CoO buffer)

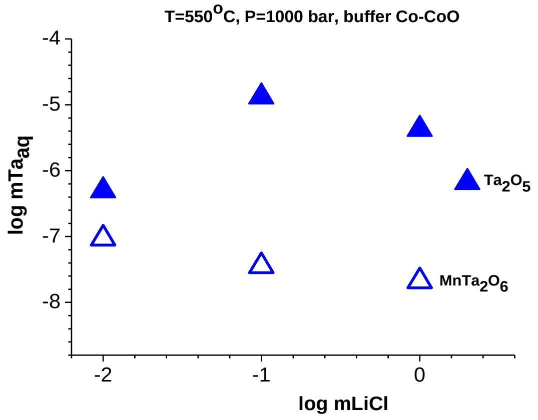

Fig.4. The solubility of Mn-tantalite and Ta_2O_5 as a function of LiCl concentration at T = 550°C, P= 1 kbar (Co-CoO buffer)

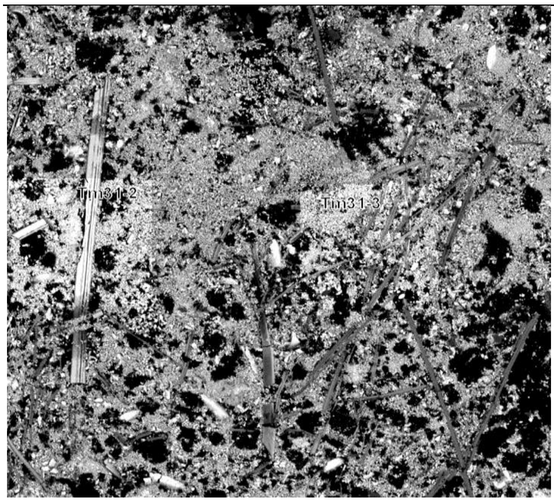

Photo 1. Golden brown needle crystals in 1m KCl (T = 550°C, P= 1 kbar, Co-CoO buffer)

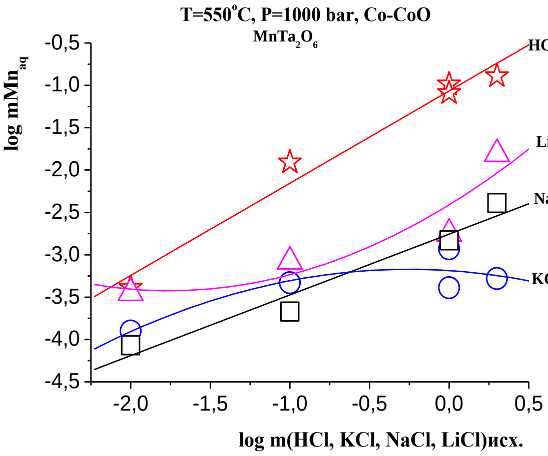

Fig.5. The solubility of Mn as a function of chloride concentration at T = 550°C, P= 1 kbar (Co-CoO buffer)

It is established that in KCl solutions, the dependence of Mn solubility on chloride concentration is not strong (Fig. 5). The study of solids run products on a microprobe detected the presence of the newly formed a golden brown needle crystals of compound with Mn and Pt, having a complex structure: K_2O-4.28%; MnO-25.87%; Ta_2O_5-4.26%; PtO-37.20%; FeO-1.74% (Fig. 1). The source of Pt is platinum capsules in which the experiment was conducted. A significant amount of manganese and some of tantalum and potassium form the new solid phase.

Based on these experiments we can conclude that in all chloride solutions (HCl, NaCl, KCl, and LiCl) the Ta solubility in equilibrium with Mn-tantalite and tantalum oxide is very low (near $10^{-7.5}$-$10^{-5.5}$ m). This is due to the fact that in all chloride solutions, Mn- tantalite dissolves incongruently. The Mn concentration in the solution is 3 to 5 orders of magnitude higher than the Ta one. This means that in the presence of Fe and Mn in the rocks hydrothermal transport of Ta in chloride solutions is practically impossible because of its low solubility. Chloride hydrothermal solutions are not capable of transferring tantalum in the amounts sufficient for the formation of commercially viable ore deposits. Comparison of the results for Mn-tantalite and Ta_2O_5 confirms the thesis that the solubility of simple oxides (Ta_2O_5 and Nb_2O_5) restricts the upper limit of these elements concentration in hydrothermal solutions.

Acknowledgements: The work was done with the financial support of the ONZ-2 Program.

Reference

1. Zaraisky G.P., V.S. Korzhinskaya, N.P. Kotova, (2010). Experimental studies of Ta_2O_5 and columbite–tantalite solubility in fluoride solutions from 300 to 550°C and 50 to 100 MPa. *Mineralogy and Petrology*, № 99, pp. 287-300.

Martynov[1] K.V., Akhmedjanova[2]G.M., Kotelnikov[2] A.R., Tananaev[1] I.G. Distribution of alkaline cations (Na, K, Cs) between kosnarite and water electrolyte solutions at elevated temperatures

[1]A.N. Frumkin Institute of Physical Chemistry and Electrochemistry RAS, Moscow
[2]Institute of Experimental Mineralogy RAS, Chernogolovka

Abstract. Na and Cs distribution between titanium and zirconium kosnarites and nitrate water solutions at a temperature 200°C was experimentally studied. On the basis of the received results and also known earlier data on Na and K cationic exchange between kosnarites and chloride solutions at 450-700°C the thermodynamic models of mixture for binary regional sections of zirconium kosnarite solid solution were constructed. On these models 200°C isotherms of alkaline cations distribution between zirconium kosnarite and salt water solutions in Na-K and K-Cs regional sections were calculated.

Key words: kosnarite, solid solution, cationic exchange, distribution isotherm.

Citation: Martynov K.V., G.M. Akhmedjanova, A.R. Kotelnikov, I.G. Tananaev(2013). Distribution of alkaline cations (Na, K, Cs) between kosnarite and water electrolyte solutions at elevated temperatures.

The reached successes in hydrothermal synthesis of crystal compounds having kosnarite mineral structure at moderate temperatures (from 90°C) open opportunity to take alkaline and alkaline-earth nuclear fission products (first of all ^{137}Cs и ^{90}Sr) directly from technological solutions by a cationic exchange method. Special value gets this method for waste of SNF pyrochemical reprocessing representing concentrated electrolytes. To apply this method, it is necessary to know nature of component distribution between liquid and solid phases. Earlier phase distribution of Na and K between solid solutions of titanium [Asabina, 2006] and zirconium [Kotelnikov, 2000] kosnarites and chloride water solutions was studied at temperatures 450-700°C and pressure of 1-2 kbar. We were faced by a task to study behavior of Cs at P-T parameters being more real for technology.

To solve an objective we experimentally studied Na and Cs distribution between Ti, $Ti_{0.5}Zr_{0.5}$ and Zr kosnarites and nitrate water solutions at a temperature 200°C and saturated vapor pressure (1.55 MPa) in autoclaves with teflon inserts. The experiments were made by a synthesis method when approaching to an isotherm from both sides using X-ray amorphous xerogels as starting materials. The technique of the xerogels preparation is described earlier [Martynov, 2012]. The solid products of experiments were studied by X-ray powder diffraction method (X-ray diffractometer Carl Zeiss URD-63, CuKα radiation, Ni-filter, λ=1.5418 Å) and electron microprobe analysis (SEM Tescan Vega II XMU with X-ray energy dispersive spectrometer Oxford Instruments INCAx-sight). The quenching solutions were analyzed by atomic absorption spectrometer with flame atomizer KORTEK KVANT-2A.

For studied Na-K-Cs system the component distributions in binary regional sections are described by following exchange reactions:

$$NaZr_2(PO_4)_3 + Cs^+ = CsZr_2(PO_4)_3 + Na^+, \tag{1}$$

$$NaTi_2(PO_4)_3 + Cs^+ = CsTi_2(PO_4)_3 + Na^+, \tag{2}$$

$$Na(Ti,Zr)_2(PO_4)_3 + Cs^+ = Cs(Ti,Zr)_2(PO_4)_3 + Na^+, \tag{3}$$

$$KZr_2(PO_4)_3 + Cs^+ = CsZr_2(PO_4)_3 + K^+, \tag{4}$$

$$NaTi_2(PO_4)_3 + K^+ = KTi_2(PO_4)_3 + Na^+ , \tag{5}$$

$$NaZr_2(PO_4)_3 + K^+ = KZr_2(PO_4)_3 + Na^+. \tag{6}$$

The mole fractions of components (minals, end-members) in the solid phases X_{ss} and water solution X_{fl} are defined as:

$$X_{ss/fl}(1)\text{-}(3) = [Cs_{ss/fl}]/([\ Cs_{ss/fl}] + [Na_{ss/fl}]), \tag{7}$$

$$X_{ss/fl}(4) = [Cs_{ss/fl}]/([\ Cs_{ss/fl}] + [K_{ss/fl}]), \tag{8}$$

$$X_{ss/fl}(5),(6) = [K_{ss/fl}]/([\ K_{ss/fl}] + [Na_{ss/fl}]). \tag{9}$$

The phase distribution coefficients are register as follows:

$$Kd(1)\text{-}(6) =\{X_{ss}/(1- X_{ss})\}\cdot\{\ (1- X_{fl})/X_{fl}\}. \tag{10}$$

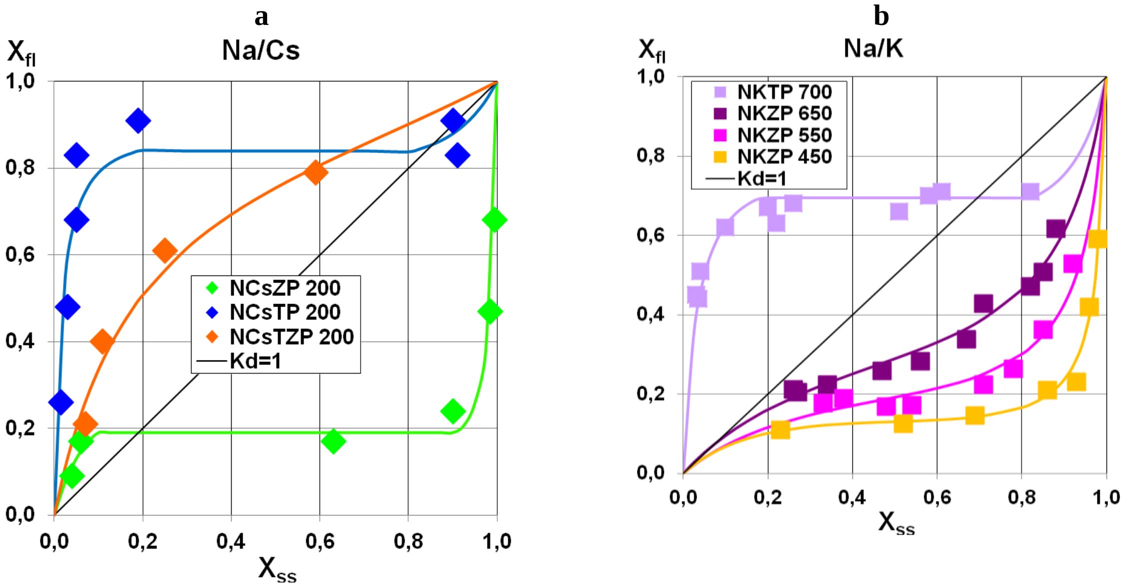

Fig. 1. The diagrams of the elements phase distribution between kosnarites and water solutions at a temperature 200°C according to our data (**a**) and 450-700°C by data [Asabina, 2006], [Kotelnikov, 2000] (**b**). Designations of solid solutions: NCsZP – $Na_{1-X}Cs_XZr_2(PO_4)_3$, NCsTP – $Na_{1-X}Cs_XTi_2(PO_4)_3$, NCsTZP – $Na_{1-X}Cs_X(Ti,Zr)_2(PO_4)_3$, KCsZP – $K_{1-X}Cs_XZr_2(PO_4)_3$, NKTP – $Na_{1-X}K_XTi_2(PO_4)_3$, NKZP – $Na_{1-X}K_XZr_2(PO_4)_3$, nearby - temperature, °C.

The results of our experiments and settlement isotherms describing them are presented in fig. 1a. Two phenomena attract attention: 1) contrast nature of the components distribution between solid and liquid phases for titanium and zirconium solid solutions, 2) existence of wide areas of immiscibility in both series, traced by horizontal sites of curves. The last one for titanium phases is accompanied by reconstructive phase transition: trigonal-rhombohedral (R -3 c) kosnarite (the compositions enriched with Na) → tetragonal phase (the compositions enriched with Cs). For zirconium solid solutions phase transition isn't shown on X-ray powder diffraction patterns. Possibly, it has more gentle dislocation disposition. It is interesting that mixed the titanium-zirconium kosnarites don't tend to decomposition of solid solution and phase transition. Despite significantly different parameters and an experimental technique, for Na and K distribution we have a similar picture (fig. 1b).

The reason of the phenomena stated above consists in crystal-chemical specific features of the solid solutions, which some manifestations for heterovalent replacements in kosnarite we studied earlier [Martynov, 2012]. In the case under consideration for simpler isovalent isomorphism the only influencing factor is a ratio of sizes of framework forming (Ti *vs* Zr) and extra frame (Na *vs* Cs&K) cations. So for distribution of components between water solutions and solid phases it is possible to notice that solid solution with a large framework forming cation (Zr) is enriched rather water solution with large extra frame cations (Cs&K). As it will be shown below, the dimensional crystal-chemical ratio is projected on thermodynamic functions of mixture of the solid solutions.

To calculate thermodynamic mixture parameters of solid solutions we used the analysis of Kd dependence from compositions of coexisting phases applied in [Martynov, 1990]. It was shown that for distribution between ideal and nonideal solutions in case lnKd linearly depends on composition of a nonideal phase:

$$\ln Kd = C_0 + C_1\cdot X, \tag{11}$$

in order that describe excess free energy of mixture of nonideal solution the one-parametrical model can be used:

$$G^e = X\cdot(1-X)\cdot W, \qquad (12)$$

$$G^e{}_X = R\cdot T\cdot \ln(\gamma_X) = (1-X)^2\cdot W, \qquad (13)$$

$$G^e{}_{1-X} = R\cdot T\cdot \ln(\gamma_{1-X}) = X^2\cdot W, \qquad (14)$$

$$G^{mix} = R\cdot T\cdot(X\cdot \ln X + (1-X)\cdot \ln(1-X)) + G^e, \qquad (15)$$

$$R\cdot T\cdot \ln Kd = -\Delta G^0 - G^e{}_X + G^e{}_{1-X}, \qquad (16)$$

the ratios are thus right:

$$\Delta G^0 = - R\cdot T\cdot(2\, C_0 + C_1)/2 \text{ and} \qquad (17)$$

$$W = R\cdot T\cdot C_1/2, \qquad (18)$$

where C_0 and C_1 – polynomial coefficients (11), W – model parameter, ΔG^0 – Gibbs free energy (isothermal-isobaric potential) of exchange reaction, G^e и $G^e{}_i$ – integral and partial excess free energy of mixture, G^{mix} - free energy of mixture, γ_i – activity coefficient of a component *i*, X and (1-X) – mole fractions of components (minals, end-members), R – universal gas constant, T – temperature K.

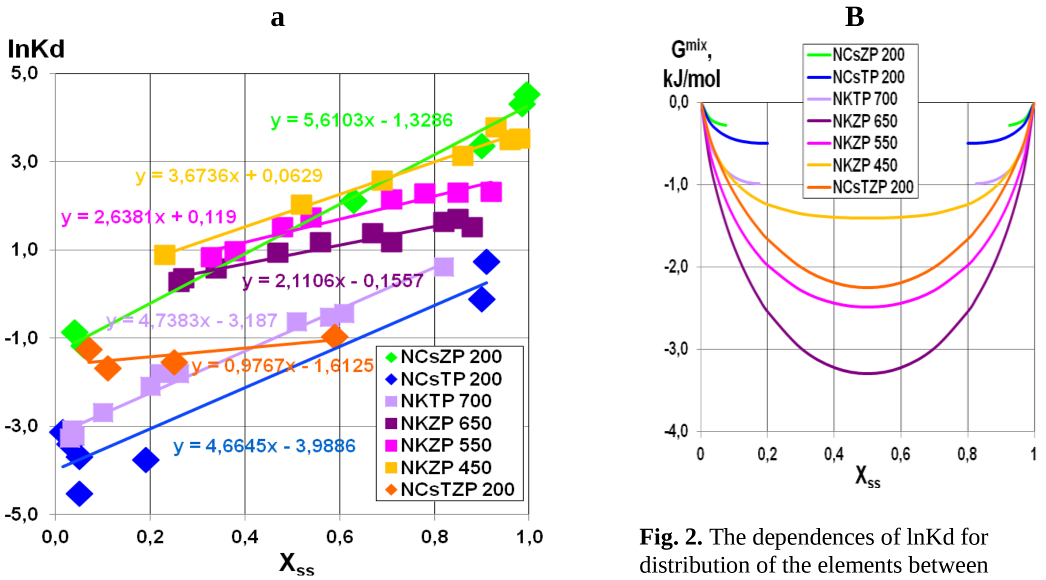

Fig. 2. The dependences of lnKd for distribution of the elements between kosnarites and water solutions (**a**) and the dependences of solid solutions free energy of mixture (**b**) from kosnarite composition.

Table 1. The values of Gibbs free energy of exchange reactions (1)-(6) and the parameters of thermodynamic mixture model for kosnarite solid solutions at the corresponding temperatures

ss t°C	NKTP 700	NKZP 650	NKZP 550	NKZP 450	NCsTP 200	NCsZP 200	NKZP 200	KCsZP 200	NCsTZP 200
ΔG^0, J/mol	6617	-6905	-9842	-11422	6516	-5809	-17306	11502	4422
W, J/mol	19169	8100	9028	11044	9175	11035	14535	-3495	1921

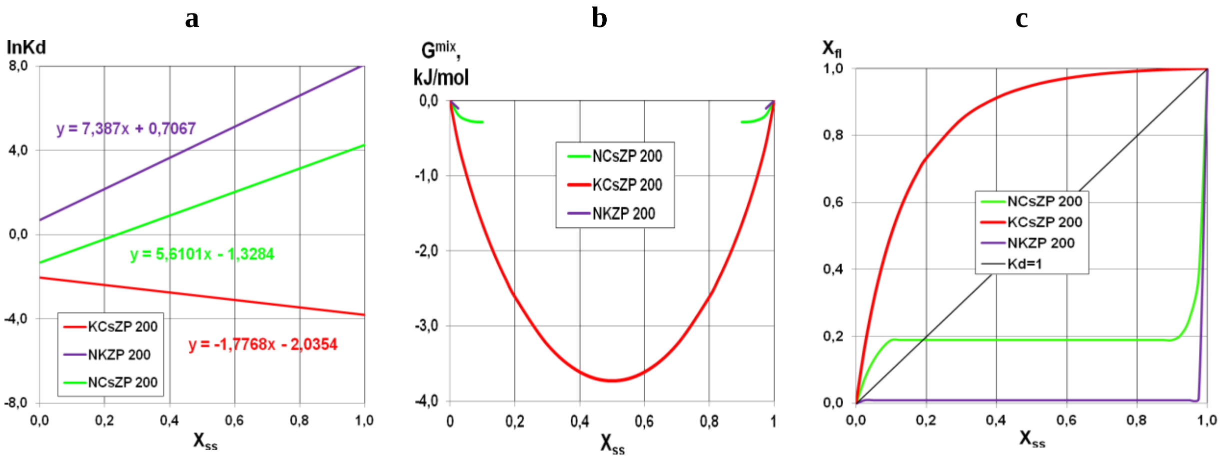

Fig. 3. The dependences of lnKd of exchange equilibria (**a**) and the dependences of solid solutions free energy of mixture (**b**) from Zr kosnarite composition and the the diagram of the elements phase distribution between Zr kosnarites and water solutions (**c**) at 200°C

The expressions approximating dependences of lnKd for distribution of elements between kosnarites and water solutions from composition of solid phases are shown in fig. 2a. The values of Gibbs free energy of exchange reactions (1)-(6) and parameters of thermodynamic mixture model for kosnarite solid solutions at the corresponding temperatures are reduced in tab. 1. The dependences of kosnarite solid solutions free energy of mixture from the composition, calculated on the offered model are presented in fig. 2b. The analysis of the obtained data testifies that all experimentally studied solid solutions have a positive deviation from ideality, i.e. possess relative instability. However, amplitude of this deviation is various both for different compositions, and for different temperatures. ΔG^0 values of exchange reactions for Ti solid solutions are positive, and for Zr – are negative. That defines prevailing nature of phase components distribution.

200°C isotherms of alkaline cations distribution between zirconium kosnarites and water solutions in Na-K and K-Cs regional sections which weren't studied experimentally were received by calculations. The first of them is calculated proceeding from values $\Delta G^0(6)$ and W_{NKZP} extrapolated linearly on temperature down to 200°C. The second one is calculated using $\Delta G^0(4)$ and W_{KCsZP} values determined by a standard method from the coefficients of an expression, describing of lnKd(4) dependence on the solid solution composition (fig. 3a), found from a ratio

$$\ln Kd(4) = \ln Kd(1) - \ln Kd(6). \qquad (19)$$

The least exact stage of these calculations is linear temperature extrapolation of parameters for Na-K section of the system. Probably thereof we received a negative deviation from ideality for KCsZP solid solution (fig. 3b) and also positive value ΔG^0 (4) (tab. 1) at 200°C. The last gives to violation of the regularity determined above of dependence of components distribution between kosnarites and water solutions from a ratio of sizes of framework forming and extra frame cations (fig. 3c). At the same time the tendencies which were shown thanks to the carried-out calculations: wide areas of immiscibility in NKZP section and high stability of KCsZP solid solution are presented quite natural from a position of crystal-chemical approach.

Conclusions

1). The kosnarite solid solutions show the most different options of phase distribution of components with water solutions of electrolytes depending on composition of a framework, a combination of extra frame cations and temperature.

2). The stability of kosnarite solid solutions, their thermodynamic parameters of mixture and nature of phase distribution of components with water solutions of electrolytes depend on a ratio of sizes of framework forming and extra frame cations.

3). The obtained data can be used for creation of cationic exchange techniques to extract of the components from water solutions of electrolytes when processing SNF both on pyrochemical, and on traditional (PUREX) technology.

This work was supported by *RF State* Contract № 16.740.11.0538 from 16.05.2011.

References :

1. Asabina, E.A. et al. (2006). Hydrothermal synthesis and characterization of $(Na,K)Ti_2(PO_4)_3$ solid solutions. *Russian Journal of Inorganic Chemistry*. Vol. 51, No 7, 988-993.
2. Kotelnikov, A.R. et al. (2000). Preparation and structural study of complex zirconium alkali metal orthophosphates. 4. Formation and thermodynamic characteristics of solid solutions in high-temperature water-salt systems. *Radiokhimiya*, Vol. 42, No 4, 325-330 (in Russian).
3. Martynov, K.V. (1990). Experimental study of Mg and Fe distribution between ankerite and breinerite solid solutions in $MgCO_3$-$CaCO_3$-$FeCO_3$ system at 250-450°C and thermodynamic properties of ankerite. *Geokhimiya*, No 12, 1688-1696 (in Russian).
4. Martynov, K.V. et al. (2012). Limits of replacement of Zr and Ti for Al in kosnarite solid solution including alkali and alkaline earth charge-compensating cations. *Vestn. Otd. nauk Zemle*, 4. NZ9001. doi:10.2205/2012NZ_ASEMPG

Mironenko [1]M.V., Polyakov [2]V.B., Marion [3]G. Calculation of equilibria in CO_2-bearing water-salt systems. Extension of FREZCHEM model

[1] V. I. Vernadsky Institute of Geochemistry and Analytical Chemistry RAS, Moscow

[2] Institute of Experimental Mineralogy RAS, Chernogolovka

[3]Desert Research Institute

Abstract. A chemical-thermodynamic model of water-salt-gas systems at low temperatures FREZCHEM has been extended to calculate formation of both gas hydrate $CO_2·6H_2O$ and liquid CO_2. The model uses Pitzer equations to calculate water activity and activity coefficients of species and Peng-Rodinson equation to calculate gas fugacities. Based on admission that hydration number of CO_2 and CH_4 gas hydrates is constant and equal to 6, the constants of formation of $CO_2·6H_2O$ and $CH_4·6H_2O$ were obtained from approximation of experimental data of phase equilibria in a wide range of PT conditions. A procedure has been described to calculate constants of the equilibrium "liquid CO_2-gaseous CO_2" with EOS of Span and Wagner (1) for pure CO_2. The results of calculation of equilibria in the system H_2O-NaCl-CO_2 are listed for various temperatures.

Key words: liquid carbon dioxide, gas hydrates, electrolyte solutions, phase equilibria.

Citation: Mironenko M.V., V.B. Polyakov, G.Marion (2013). Calculation of equilibria in CO_2-bearing water-salt systems. Extension of FREZCHEM model.

A chemical-thermodynamic model FREZCHEM has been designed for computation equilibria in water-salts-gas systems within temperature range of -100 ÷ 25° C and pressures of 0.5 ÷ 2000 bar. The model uses a data base which includes temperature dependencies of equilibrium constants of chemical reactions and volumetric properties of components, as well as temperature and pressure dependencies of Pitzer interaction parameters. Independent components are as following Na^+-K^+-Ca^{2+}-Mg^{2+}-FeII-FeIII-Al^{3+}- H^+-OH^-- Cl^- - SO_4^{2-} - NO_3^-- ClO_4^-- NH_3-CO_2 – CH_4-$H_4SiO_4^0$-O_2. Hydrolysis and complex formation are taken into account [Marion et al., 2009].

We calculate chemical equilibria using Gibbs free energy minimization. Water activity and activity coefficients of aqueous species are calculated with Pitzer model, and compressibility and fugacity coefficients of a gas solution with Peng-Robinson equation.

The paper documents extension of the model for CO_2-containing water-salt systems.

1. Gas hydrate $CO_2{\cdot}6H_2O(cr)$. Recently G. Marion et al. introduced a chemical-thermodynamic calculation of possibility of formation of gas hydrates $CO_2{\cdot}6H_2O$ and $CH_4{\cdot}6H_2O$ and their solid solution (Marion et al., 2006). It is well known that compositions of even pure hydrates of CO_2 and CH_4 depend on temperature and pressure. It was postulated that a hydration number N is constant and equal to *6*. (Theoretical models predict for hydrates of CO_2 и CH_4 (Structure I) hydration numers N from 5.9 to 6.3 [Bakker et al., 1996]). Molar volumes of both hydrates are the same and equal to 135.75 cm^3/mole (Sloan, 1988).

G. Marion approximated experimental data from (6) on CH_4 and CO_2 gas hydrate equilibria in water-gas systems at T= 180÷298 K with Krichevsky equation:

$$\ln\left(\frac{K^P}{K^{P0}}\right) = \left(-\frac{\Delta V_r^0\left(P-P^0\right)}{RT} + \frac{\Delta \bar{K}_r^0\left(P-P^0\right)^2}{RT}\right)$$

As a result, temperature dependencies of a constant $K^{P0}_{CO_2 \cdot 6H_2O} = f_{CO_2(g)} \cdot a_w^6$ of the reaction $CO_2{\cdot}6H_2O(cr) = CO_2(g) + 6H_2O(l)$ and $K^{P0}_{CH4 \cdot 6H_2O} = f_{CH_4(g)} \cdot a_w^6$ of the reaction $CH_4{\cdot}6H_2O(cr) = CH_4(g) + 6H_2O(l)$ were obtained (Marion et al., 2006). Calculations of equilibria in systems “electrolyte solutions- CO_2” with obtained constants showed a good agreement with available experimental data [Englezos and Hall, 1994].

As an example of modeling formation of $(CO_2,CH_4){\cdot}6H_2O(cr\ )$ gas hydrate solid solution in equilibrium with mixed electrolyte solution, a calculation of freezing the system “1 kg H_2O +1 mole NaCl+0.1 mole KCl+0.01 mole $CaCl_2$” at P_{tot}=10 bar, fCO_2=4.5 bar, and fCH_4=4.5 bar is shown in fig.2.

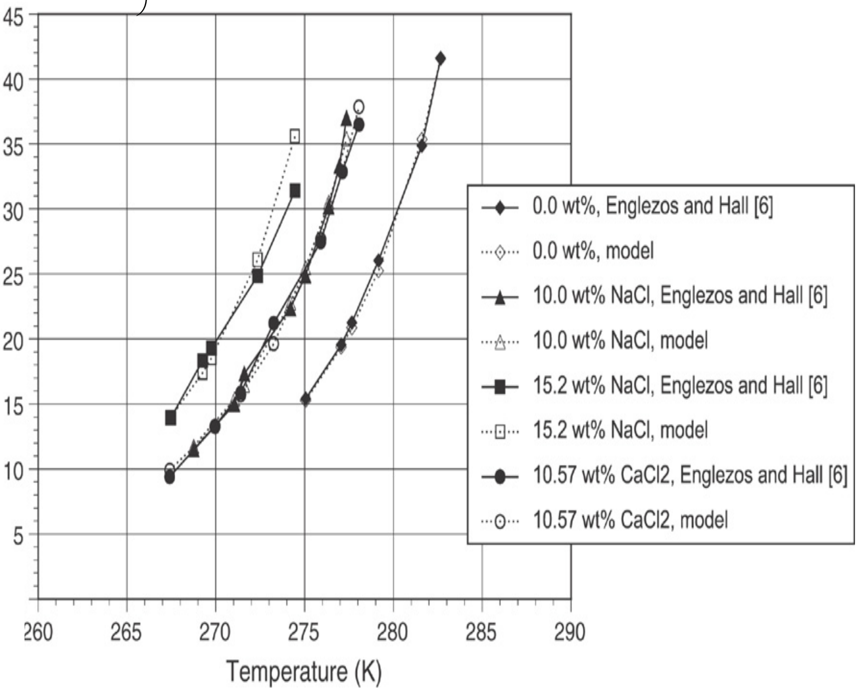

Fig. 1. Calculated and experimental saturation curves $CO_2{\cdot}6H_2O$ (cr) with various electrolyte solutions.

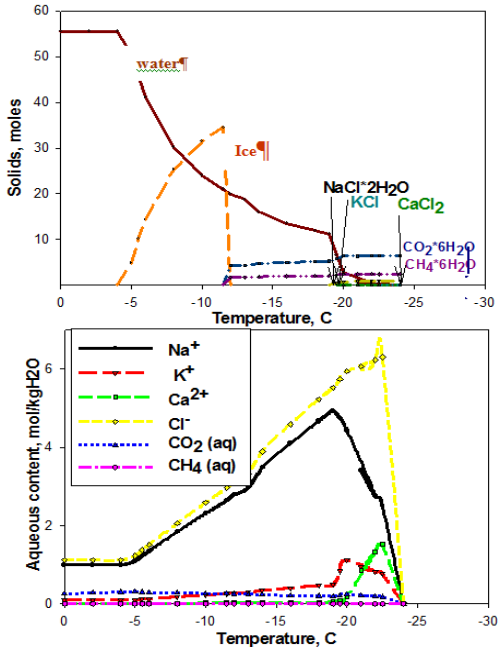

Fig. 2. Modeling freezing the system “1 kg H_2O + 1 mole NaCl + 0.1 mole KCl + 0.01 mole $CaCl_2$” at P_{tot}=10 bar, fCO_2=4.5 bar, fCH_4=4.5 bar.

2. Liquid carbon dioxide. To calculate thermodynamic properties of liquid CO_2 at current T and P, and of ideal gaseous CO_2 at current temperature and standard pressure, we implanted into the equilibrium computation module a program, which calculates thermodynamic properties using a fundamental equation of state of Span and Wagner for pure carbon dioxide [Span and Wagner, 1996]. For current temperature and pressure the program determines a phase state of CO_2 in a one-component system. If T and P correspond to stability field of liquid CO_2, $G_{CO2Liquid}(T,P)$ and $G^0_{CO2Gas}(T,1)$ are calculated. Formats of a data base FREZCHEM demand of values of equilibrium constants of reactions of component formation. An equilibrium constant of a reaction CO2(gas)=CO2(liquid) can be calculated as

$$\ln K_{T,P} = \frac{G_{CO2Liquid}(T,P) - G^0_{CO2Gas}(T,P)}{RT},$$

where $G^0_{CO2Gas}(T,P) = G^0_{CO2Gas}(T,1) + RT\ln(P)$ is Gibbs energy of formation of a hypothetic ideal gas CO_2 for current T and P.

Further, during calculating point chemical equilibria in the system, liquid carbon dioxide is supposed as a one-component solid (as salts and ice), and fugacities of CO_2 in a carbon dioxide-steam gaseous solution are calculated with Peng-Robinson equation of state

One can see in fig.3 calculated phase compositions of the system "1 kg H_2O + 3 moles NaCl + 10 moles CO_2" at various temperatures and at pressure of 50 bar on a diagram, plotted by Akinfiev and Diamond using their equation of state of the system H_2O-NaCl-CO_2 [Akinfiev and Diamond, 2010]. Phase compositions are the same.

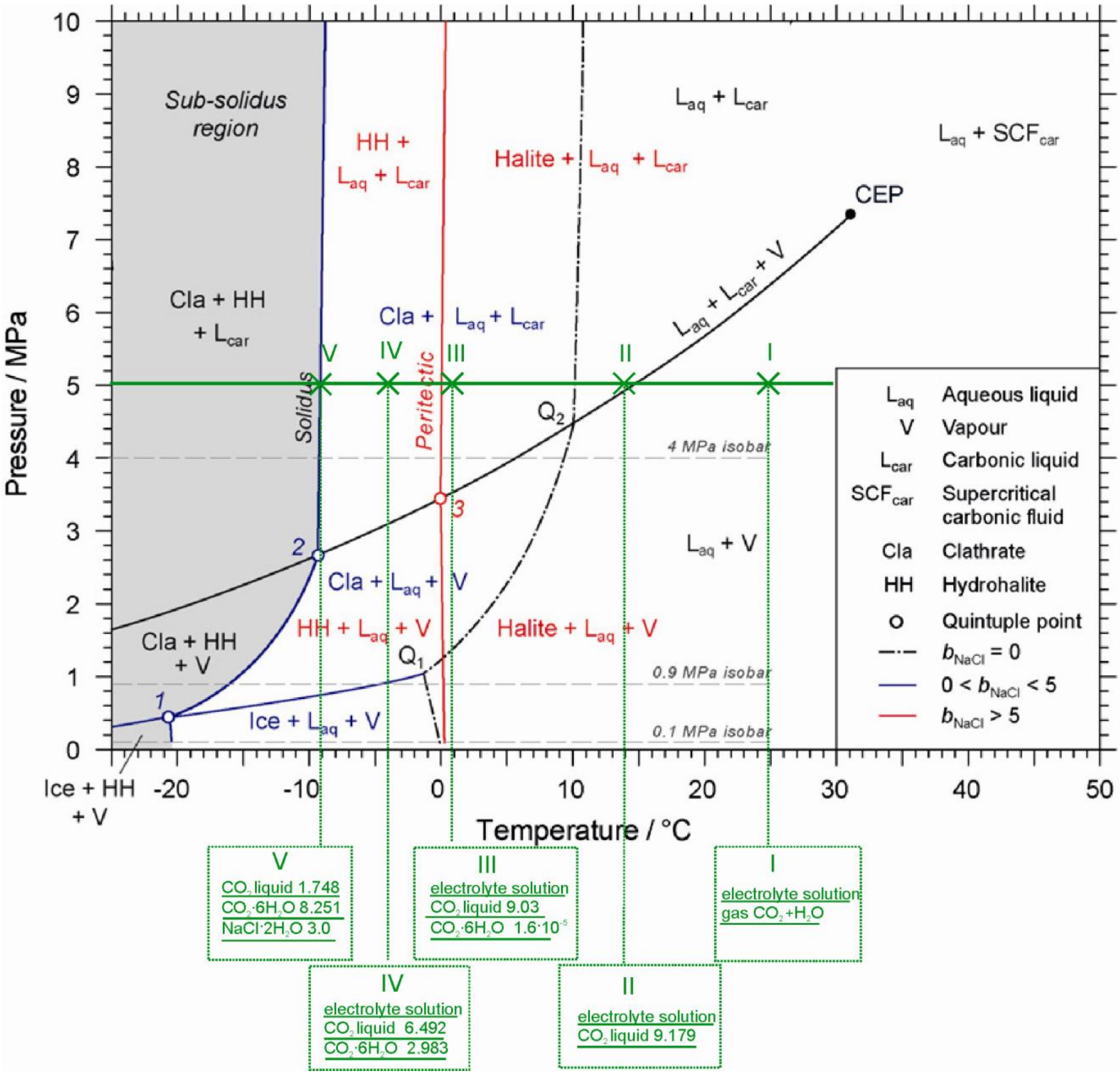

Fig. 3. Calculated phase compositions of the system "1 kg H_2O + 3 moles NaCl + 10 moles CO_2", on the diagram of state of the system "H_2O-NaCl-CO_2" from [Akinfiev and Diamond,2010].

Table 1. Equilibrium composition of the system “1 kg H_2O + 3 moles NaCl + 10 moles CO_2” at P=50 bar and T=-4ºC

```
TEMPERATURE   -4.00 C (269.15 K)   PRESSURE   50.000 bar

                 ONE COMPONENT SOLIDS AND LIQUIDS
 N    PHASE                 MOLE          deltaG/RT    V, cm3
   1 CO2*6H2O(cr)           2.983131     -40.0437     404.960
   2 CO2(liquid)            6.492195     -39.0710     296.305
                VOLUME OF SOLIDS  701.265 cm3
                          AQUEOUS SOLUTION
                    IONIC STRENGTH   4.428
                  OSMOTIC COEFFICIENT    1.1615
  N   SPECIES              MOLE        MOLALITY     ACTIVITY     ACT.COEFF.   -del(G/RT)
   1 Na+               0.30000E+01  0.44278E+01  0.36845E+01   0.8321     -0.0083
   2 H+                0.41449E-03  0.61175E-03  0.18762E-02   3.0670      0.0000
   3 Cl-               0.30000E+01  0.44278E+01  0.33024E+01   0.7458      0.0352
   4 OH-               0.54822E-11  0.80913E-11  0.35400E-12   0.0438     34.7858
   5 HCO3-             0.41449E-03  0.61175E-03  0.23032E-03   0.3765    -24.5786
   6 CO3-2             0.73835E-10  0.10898E-09  0.26541E-11   0.0244     -0.0213
   7 CO2,aq            0.52426E+00  0.77377E+00  0.21343E+01   2.7583    -39.8291
   8 H2O(l)            0.37609E+02               0.81749E+00               0.0394
                          pH= 2.727
                    DENSITY    1.1682      VOLUME   749.862 cm3
```

In table 1 a calculated equilibrium composition of the system at P=50 bar and T=-4ºC (point IV in fig. 3) is shown in detail.

Thus, the proposed approach gives possibility to calculate phase compositions of systems “electrolyte solution – CO_2” using methods of chemical-thermodynamic modeling. An aqueous solution may be a mixture of electrolyte solutions; pH is calculated as well as a hydrolysis of CO_2 (aq). The approach can be extended for systems with many gases.

The study was partly supported by Russian Foundation for Basic Research, Project 11-05-00780.

References :

1. Akinfiev N.N., L.W. Diamond (2010). Thermodynamic model of aqueous CO_2–H_2O–NaCl solutions from −22 to 100 C and from 0.1 to 100MPa. *Fluid Phase Equilibria*, 295, 104–124.
2. Bakker R. J., J. Dubessy, M. Cathelineau (1996). Imorovements in clathrate modeling. 1.The H_2O-CO_2 system with various salts *Geochim.Cosmochim.Acta*, 60, 1657-1681.
3. Englezos P., S. Hall (1994). Phase equilibrium data on carbon dioxide hydrate in the presence of electrolytes, water soluble polymers and montmorillonite,Can. *J. Chem. Eng.*, 72, 887–893.
4. Marion G. M., M. V.Mironenko, M. W.Roberts (2009). FREZCHEM: A geochemical model for cold aqueous solutions. *Computers and Geosciences*, doi:10.1016/j.cageo.2009.06.004
5. Marion G. M., D. C. Catling, J. S. Kargel (2006). Modeling gas hydrate equilibria in electrolyte solutions. *Computer coupling of phase diagrams and thermochemistry*, 30, 248-259
6. Sloan E.D. Jr (1988) Clathrate hydrates of natural gases, second edn. Marcel Dekker, New York,.
7. Span R., W. Wagner (1996). A New equation of state for carbon dioxide covering the fluid region from the triple-point temperature to 1100 K at pressures up to 800 MPa. *J. Phys. Chem. Ref. Data*, 25, 1509–1596.

Plyusnina L.P., Kuz’mina T.V., Likhoidov G.G. Interaction of platinum with carbonaceous matter and sulphur (200-400^{o}C, 1 kb)

Far East Geological Institute, Vladivostok

Abstract. In connection with the problem of platinum discovery and analysis in carbon-bearing rocks, the experimental study of the Pt±Fe±S-C-H_2O systems was performed. The first quantitative information about Pt sorption on carbonaceous matter in the presence of sulfur and its accelerating of the aromatization processes were obtained. The “armoring” effect by carbonaceous multi-layering films deposited on Pt surface was observed. Measured by SEM the C-Pt-O-S variable compositions of the films suppose an existence of the platinum-organic complexes preceding Pt crystallization. An absence of sulfur in the new-formed Pt-C phases along with cooperite in run products explains its rare occurrences in the black shales.

Key words: Platinum, carbonaceous matter, sulfur, sorption.

Citation: Plyusnina L.P., T.V. Kuz’mina, G.G. Likhoidov (2013). Interaction of platinum with carbonaceous matter and sulphur (200-400ºC, 1 kb).

Discovery of platinum group elements (PGE) in golden and copper deposits of black shale attracts more and more attention [Kucha, 1982, Ermolaev et al., 1995, Distler et al., 1996]. Multiple mineral forms of PGE include native metals, intermetallides, sulphides, arsenides, and presumably, metallorganic compounds. The lasts were confirmed experimentally [Plyusnina et al., 1999] and were found in the volcano Kudriavyi sublimates [Distler et al., 2008]. In the Pt-C-H_2O system (at 25-400^{o}C 1 kb) sorption capacity of soluble hydrocarbons and kerogen in relation to Pt was measured for the first time [Plyusnina et al., 1999].

Sulphur in native and sulphide forms usually presents in black shales. The main of platinum is connected, for example, with pyrite and arsenopyrite at the Natalka deposit of Magadan district [Plyusnina et al., 2003]. So, elucidation of the sulfur effect on Pt sorption offers doubtless interest. Performed before, experimental study of Au sorption by bitumen in S-bearing systems illustrated the influence of elemental and sulphide forms of sulfur under discussion [Plyusnina et al., 2009; 2012]. Solubility of Pt in the presence of sulphide sulfur (the Pt-Fe-S-H_2O system) differs from Au one notably [Plyusnina et al., 2007], that may define a specificity of the noble metals (NM) sorption on carbonaceous matter (CM).

Runs at 200, 300 and 400°C (P_{tot} = 1 kb) are performed in Pt ampoules (10×100×0.2 mm) placed in Ti-Ni alloy autoclaves of 20 cm^3 useful capacity. Total pressure assigns by doubly distilled water in accordance with the P-V-T relation. Asphaltenes (50 mg) fractionated from brown coal of Pavlovskoe deposit, Prymorie, were simulated CM. The source of Pt was walls of ampoules dissolved under the experimental conditions [Plyusnina et al., 1999]. The source of sulfur in runs was elemental sulfur (10 mg) or natural pyrite (30 mg). Each isothermal series included 12 runs (in 4 autoclaves with 3 runs of the systems). Runs duration equals 40-14 days at 200-400°C, accordingly. After runs quenching, the water fraction (WF) from autoclave was filtered, and the precipitate of CM was separated in an alcohol-benzene mixture at 50°C, for 12-20 hrs in the soluble fraction (SF) and an insoluble soot-like residue (IR or kerogen). The CM of both fractions was decomposed by heating in concentrated inorganic acids and transferred to wet salts [Plyusnina et al., 1999; 2012]. From them Pt was extracted by alkylaniline and measured using atomic absorption spectrophotometer with thermoelectric atomization (Shimadzu AA-6800, at a sensitivity of 0.002 ppm). Kerogen and SF are studied using IR-spectrophotometer Nicolet 6700.

The Pt content is minimal in WF, rises in a few orders in SF, and riches maximum in kerogen (IR) (tab. 1). Temperature and system composition affect the change of Pt content values within an uncertainty interval. The necessity to analyze of maximal Pt content in kerogen requires, because of the high apparatus sensitivity, essential dilution of starting solutions that result in the raising uncertainty interval (±0.3-0.45 log mPt).

The mechanism of metal sorption depends on composition and molecular structure of CM [Varshal et al., 1996]. The absorbance bands 880-875, 966-974, 1037, 1083 cm^{-1} of IR-spectra of SF and kerogen, appear at 400°C in the S-bearing systems (tabs. 2 and 3), and may present C-S and S-H bonds. The IR-spectra of kerogen suggest a greater extent of degassing, aromatization and condensation than those of SF. It needs to note that kerogen concentrates the Pt at decreasing the carbonyl and carboxyl groups and C-C bonds predominance of aromatic rings (tab. 3).

After the runs in the Pt-C-H_2O, Pt-C-S-H_2O systems inner ampoule walls are covered by dark films (3-10 μm thick). The last have a strong resemblance to cooperite films, formed at 300-500°C in runs with Pt-Fe-S-O-H system without CM [Plyusnina at al., 2007]. Analysis of the films by scanning electronic microscope (EVO-50XVP) found out their essentially carbonaceous composition (mass %): C - 31.09-85.36, Pt - 8.46-67.90, S - 0-3.42, O - 0-2.77, and micro globular texture (fig. 1). On the films there are some dark spots without the micro globular texture and byt maximal sulfur content. It may points to the fluid heterogeneity at the run conditions. Pt presence in the film compositions may be result of an influence of Pt ampoule walls, and also of new formed platinum organic compounds generation. The indirect evidence of the lasts is vermicular micro tubes crystallization at 400°C (fig. 2). In spite of the tubes being separated from ampoule walls by the films, its Pt content is above (% wt.): Pt – 81.46, C - 18.54, whereas sulfur and oxygen peculiar to films are absent.

Table 1. Averaged Pt concentration (log mPt)

System	200°C			300°C			400°C		
	WF	SF*	IR*	WF	SF*	IR*	WF	SF*	IR*
C-O-H-Pt	< -8	-3.91	-4.30	-8.34	-4.47	-2.79	-7.64	-4.57	-2.36
C-S-O-H-Pt		-3.61	-3.23	-8.49	-5.21	-2.85	-7.27	-4.30	-2.51
C-S-Fe-O-H-Pt		-3.72	-2.88	-8.36	-5.21	-2.53	-7.34	-4.37	-2.41

* - concentration measured per 1 kg of dry matter.

Table 2. Infrared absorption spectra (SF, 200°C, 1 kb)

Wavenumber, cm^{-1}			Functional groups
C-O-H-Pt	C-S-O-H-Pt	C-S-Fe-O-H-Pt	
571 w	467 w	467 w	C-C, C-H (Ar)*
671 w	618 w	671 w	C-C, C-H (Ar)
722 w	722 w	721 w	C-C, C-H (Ar)
-	872 w	872 w	C-H, C-S (Ar)
1067 m	1067 m	1064 m	C-O-C
1166 w	1168 w	1158 w	C-O-C
1266 w	1266 w	1266 w	CH_2 (Ал)
1462 m	1462 m	1461 m	COO^-, C=O, CH_2 (Al)
1624 m	1628 m	1624 m	COO^-, CH_3, CH_2 (Ar)
1708 s	1707 s	1708 m	C=O
2852 s	2851 s	2852 s	CH_3, CH_2 (Al)
2921 s	2920 s	2921 s	$CH_{2,}$ CH_3 (Al)
3432 s	3412 s	3418 s	H_2O, OH^-

* Here and in tab. 3: Ar and Al denote aromatic and aliphatic functional groups;intensities: w, weak; m. medium: and s. strong.

Table 3. Infrared absorption spectra (kerogen, 200°C, 1 kb)

Wavenumber, cm^{-1}			Functional groups
C-O-H-Pt	C-S-O-H-Pt	C-S-Fe-O-H-Pt	
423 w	424 w	418 w	C-C, C-H (Ar)
673 m	673 m	673 m	C-C, C-H (Ar)
-	880 w	875 w	C-C, C-H, C-S (Ar)
1071 w	1049 m	1068 m	C=O (Ar); CHOH
-	-	1112 w	C-S, CH (Ar)
-	1159 w	1158 w	C-S, CH (Ar)
1164 w	-	1165 w	C-O-C
1270 w	-	1268 w	CH_2 (Al)
1377 w	1371 w	1373 w	CH_3 (Al)
1458 m	1456 m	1455 m	COO-, COOH, CH_3
1624 s	1624 m	1622 s	C=O, COO^-, COOH
1660 m	1660 m	1660 m	C-H (Ar)
2853 m	2854 m	2853 m	CH_2 (Al)
2923 s	2924 m	2923 s	CH_3, CH_2 (Al)
3432 s	3432 s	3432 s	H_2O, OH^-

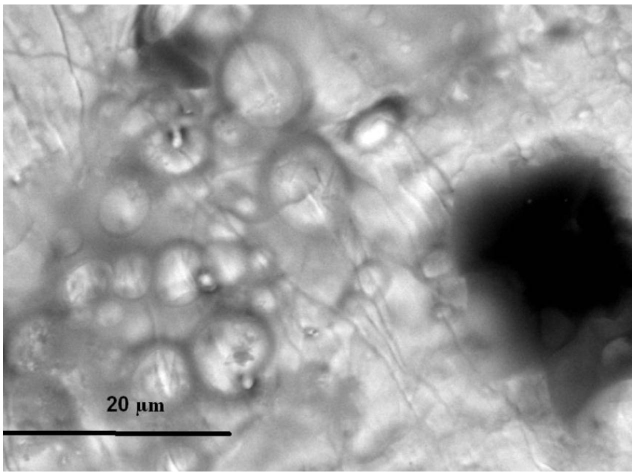

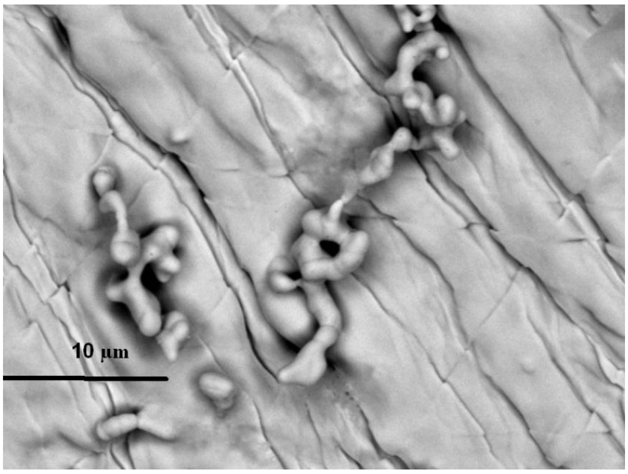

Fig. 1. Micro globular texture of the film.
Fig. 2. Pt-bearing micro tubular formations.

We did not find the cooperite (PtS), which might be connected with low Pt content in the solutions of systems with CM. So Pt content in aqueous solution of the Pt-S-Fe-O-H system (without CM) at 400°C is greater by 2-3 orders than in the CM presence [Plyusnina et al., 2007]. Moreover the lack of cooperite may be explained by sulfur deficiency owing to its interaction with the CM. The native Pt and PGE intermetallides predominate in the black shales [Distler et al., 1996], thus the experiments offer one more mechanism for rare cooperite findings in the case. It is known that cooperite in black shales usually connects with overprinting of hydrothermal sulfidization [Plyusnina et al., 2003].

In conclusion it can be point out: the results confirm acceleration of CM condensation and aromatization processes under the influence of the sulfur. It can be established that rising temperature reduces the quantity of oxygen-bearing groups in a kerogen and soluble bitumen. The increase of benzene ring valency bonds at their dehydration leads to vacancy appearance for metal adjunction. Early the same was established for Au bearing systems [Plyusnina et al., 2009; 2012]. As distinct from the last, at systems with Pt S-bearing functional groups occur in kerogen and soluble bitumen. More over, at inner Pt-ampoule surface carbonaceous films of variable composition were formed (figs. 2, 3). The absence of such films in the systems with Au may be related with more effective (by 1.5 – 2.5 times) Pt cluster interaction with graphene [Medkov et al., 2010]. Such Pt surfaces “armored” by CM explain the trouble with platinum disclosure and analyses in black shales.

We thank the Far East branch of RAS presidium for financial support of 12-3-A-08-154 and 12-2-СУ-08-011 projects.

References:

1. Kucha H. (1982). Platinum group metals in the Zechstein Cooper deposit, Poland. *Econ. Geol.*, V. 77, pp. 1578-1591.
2. Ermolaev I.N., N.A. Sosinov, V.A. Chinenov et al., (1995). The mode of platinum group metals presence in golden ore of black shale. *Geochemisty*, No 4, pp. 524-539. (in Russian)
3. Distler V.V., G.L. Mitrofanov, V.K. Nemerov et al. (1996). The mode of platinum group metals presence and its origin in gold deposit Sukhoi Log. *Geology of Ore Deposit.*, No 6, pp. 467-484. (in Russian)
4. Plyusnina L.P., T.V. Kuzmina (1999). Experimental investigation of platinum concentration by bitumen at 200-

400°C and 1 Kbar. *Geochemistry Intern.*, V. 37, No 5, pp. 441-449.

5. Distler V. V., Yu. P. Dikov, M. A. Yudovskaya et al. (2008). Platinum–chlorine–phosphorus–hydrocarbon complex in volcanic fluids: the first find in the terrestrial environment. *Doklady Earth Sciences*, V. 420, No. 4, pp. 628–631. DOI: 10.1134/S1028334X08040223
6. Plyusnina L,P., A.I. Khanchuk, V.I. Goncharov et al. (2003). Gold, platinum and palladium in Natalka ore deposit (Upper-Kolymskii region). *Doklady Earth Sciences*, V. 391, № 3, pp. 383-387. (in Russian)
7. Plyusnina L.P., T.V. Kuz'mina, G.G. Likhoidov (2009). The influence of sulfur on chemisorption of gold by carbonaceous matter at 200-400°C and P_{tot} = 1 kb. *Doklady Earth Science*, V. 429, No 6, pp. 806-808. DOI: 10.1134/S1028334X09090372
8. Plyusnina L.P., T.V. Kuz'mina, & G.G. Likhoidov (2012). Experimental Study of the Influence of Sulfur on Gold Sorption by Bitumen at 200–400°C and 1 kbar Pressure. *Geochemistry Intern.*, V. 50, No. 1, pp. 26–33. DOI: 10.1134/S0016702912010119
9. Plyusnina L.P., G.G. Likhoidov, Zh.A. Shcheka (2007). Experimental modeling of platinum behavior under hydrothermal conditions (300–500°C and 1 kbar). *Geochemistry Intern.*, V. 45, No. 11, pp. 1124–1130. DOI: 10.1134/S0016702907110055
10. Varshal G.M., T.K. Velyukhanova, A.V. Korochentsev et al. (1996). The relations between the sorption capacity of carbonaceous material in rocks for noble metals and its structure. *Geochemistry Intern.*, V. 33, pp. 139-146.
11. Medkov M.A., A.I. Khanchuk, A.V. Voit, et al. (2010). Quantum–chemical study of the interaction between Au(0), Pt(0), Ag(0) and fragments of graphenes modeling graphite structure. *Doklady Earth Sciences*, V. 434, pt 2. pp. 1321–1324. DOI: 10.1134/S1028334X10100077

Redkin A.F., Kotova N.P. Experimental study of microlyte solubility dependence from NaF concentration in aqueous solution at 800°C, 230 MPa

Institute of Experimental Mineralogy RAS, Chernogolovka

Abstact. The microlite solubility (in the presence of fluorite) is measured in the solutions containing from 0 to 46 wt.% of NaF. Thermodynamic calculations show that the data on solubility in a homogeneous region of H_2O-NaF solutions can be described in three predominant particles: $Ta_2O_5^{\circ}$, $Na_2Ta_2O_6^{\circ}$, and $Na_6H_2Ta_6O_{19}^{\circ}$. At transition to the immiscibility region one observes an anomalous behavior of the solubility curve associated with separation of the solution into two fluid phases (L_1 and L_2) of various acidity. For the first time, the NaF concentrations were evaluated in L_1 (12±1 wt.%) and L_2 (25±1 wt.%) fluid phases at 800 ° C and 230 MPa.

Key words: experiment, microlite, immiscibility region.

Citation: Redkin A.F., N.P. Kotova (2013). Experimental study of microlite solubility dependence from NaF concentration in aqueous solutios at 800°C , 230 MPa. Electron. Scien. - Inform. J. "Vestn. Otd. nauk Zemle RAN", No

The immiscibility region of water-salt solution at high P-T parameters is of interest to describe the mobilization of the poorly soluble ore components of the magmatic melts. Depending on the salt composition the immiscibility region is shown or at relatively low (sodium and potassium chlorides) or high (tantalume and lithium fluorides) fluid pressures. In this connection the magmatic source of the ore material is considered as the near-surface (depth of 3 km) or deep (depth over 7 km). Kotelnikova and Kotelnikov [Kotelnikova & Kotelnikov, 2008] consider that at the T>760 ° C and P=200 MPa, i.e. above point Q, there exists a region of fluid immiscibility where one of fluid phases (L_2) can have high concentrations of NaF salt. In the supercritical region such solution is seen as a potentially ore-bearing, but the compositions of L_1 and L_2 coexisting phases in the immiscibility region, located above the Q critical point, are not known. Peretyazhko [Peretyazhko, 2008] considered a general view of the H_2O-NaF phase diagram. According to these data, the NaF concentration at Q-point is 20-30 wt. %. Experimental data on the ore components solubility in the complex system melt Li-F-granite melt-fluoride solution indicates that the isothermal cross section of the phase fluid immiscibility may have the form shown in Fig. 1.

The purpose of our experiments to provide data on the microlite $(CaNa)Ta_2O_6F$ solubility in the NaF-H_2O system of P-Q type in a wide range of sodium fluoride concentrations and on the basis of the data to determine the boundaries of the immiscibility of water-salt solution under the above physico-chemical parameters. The feature of the technique selected is that microlite has low solubility (<10^{-4} mol/kg H_2O). So it can not have a noticeable effect on the coexisting fluid phases (L_1 and L_2) compositions in the immiscible region of the NaF-H_2O-water-salt system.

For these experiments we used microlite (Mic), obtained by hydrothermal synthesis at 800°C and P = 200 MPa. X-ray diagrams of synthesis products are fully corresponded to the standard microlite (PDF 18-1873) and pyrochlore (PDF17-0746). Microlites with the line 2Θ = 45.5° (NaF) detected, were additionally washed from NaF. We do not exclude that in the synthetic microlite the trace amounts of fluorite could be present, which were not identified on X-rays diagrams. The solutions with the NaF concentration <1 mol/kg H_2O, were directly injected into Pt capsules. To prepare more concentrated solutions the charge of solid NaF and the water were separately sealed into capsules. Presently the experiments were performed in the NaF solutions with concentrations from 0 (pure water) to 20 *m*NaF. The ratio of microlite charge to the solution was from 15/150 to 15/200. Run duration was usually 7-9 days that was sufficient to establish to balance between microlite and the acting solution.

As would be expected, microlite had low solubility for the range of NaF concentration considered in this study. The results are shown in Fig. 2. Tantalum as well as niobium, even at low concentrations, tends to form the polyoxometalates ($H_xMe_6O_{19}^{x-8}$). Despite high fluorine concentration in the solutions, the probability of fluoride complexes formation in near-neutral and weakly alkaline solutions at high temperatures is estimated as problematic [Wood, 2005]. According to available data [Prasad, 1995, Tytko, 1999] at room temperature Nb and Ta should be preferably presented by particles $Me_2O_5^{\circ}$, MeO_3^{-}, $Me_6O_{19}^{8-}$. The formation of charged particles at 800°C and P = 230 MPa, also seems unlikely.

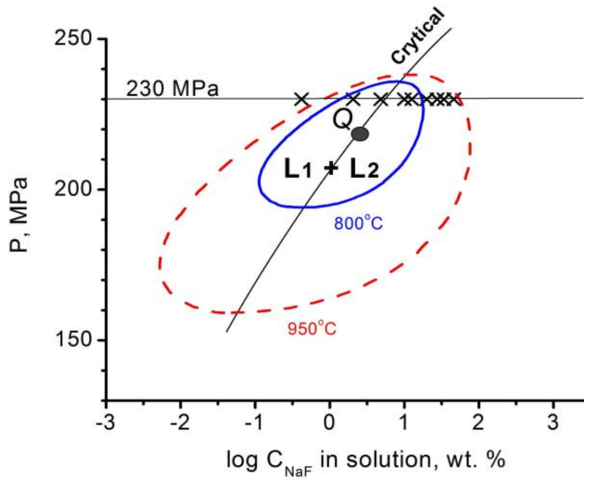

Fig.1. The cross sections of the phase diagram of fluid H_2O-NaF at constant T (800 and 950°C) according to our views. The solution compositions are shown by crosses in experiments at 800°C and 230 MPa.

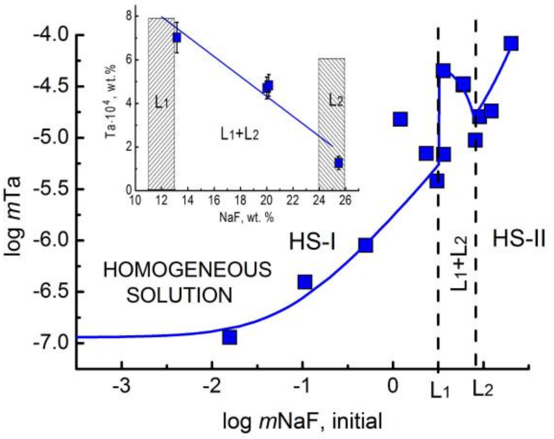

Fig.2. Experimental data on the microlite $(NaCa)Ta_2O_6F$ solubility in NaF solutions at 800°C and 230 MPa in mol/kg H_2O logarithmic coordinates. HS-I – a homogeneous solution before L_1; HS-II – salt solution after L_2.

In a homogeneous region of NaF solutions with concentrations from 0.1 to 3 mol/kg H_2O and then from 8 to 20 mol/kg H_2O (Fig. 2), the change trend of *m*Ta from *m*NaF and the water mole fraction X (H_2O) corresponds to the equation

$$mTa= =1.14\times10^{-7}+1.61\times10^{-6}\times mNaF+7.3454\times10^{-9}\times(mNaF)^3\times X(H_2O)$$

and reactions

$$(NaCa)Ta_2O_6Fcr + 2H_2O= HF + Ca(OH)_2aq + NaOHaq + Ta_2O_5^oaq \quad (0),$$

$$(NaCa)Ta_2O_6Fcr + NaF°aq = CaF_2cr + Na_2Ta_2O_6°aq \quad (1),$$

$$3(NaCa)Ta_2O_6Fcr + 3NaF°aq + H_2O= 3CaF_2cr + Na_6H_2Ta_6O_{19}^o \quad (2).$$

The highest Ta concentration ($5\cdot10^{-5}$ моль/кг H_2O) was detected in L_1 phase (3.2*m*NaF). In the range from 3.2 to 8 mol/kg H_2O the microlite solubility linearly decreases with increasing NaF concentration (in wt.%: $C_{Ta} = 13.46 - 0.457 \times C_{NaF}$), reaching a minimum ($1.5\cdot10^{-5}$ mol/kg H_2O) in a point corresponding to L_2 phase composition (8*m*NaF). Such a variation of the microlite apparent solubility with fluorite is determined by the lever rule. The discrete nature of the microlite solubility curve in the immiscibility region is connected with the decomposition peculiarities of NaF-H_2O fluid - by L_1 phase containing excess HF, and L_2 phase containing excess NaOH. The concentration of HF in the L_1 phase must exceed 0.01 mol/kg H_2O, in order to could have been formed the tantalum oxyfluoride complexes.

$$(NaCa)Ta_2O_6Fcr + NaF°aq + 2HF = CaF_2cr + 2NaHTaO_3F^o \quad (3).$$

Our studies showed that the microlite solubility, of the most important Ta-containing ore mineral, is not more than 10^{-4} mole/kg H_2O, even in highly concentrated fluoride solutions. Therefore, the most probable mechanism of the tantalum ore formation is the accumulation of tantalum in the residual melt during the long crystallization of magmatic melt. It is not preclude the possibility of tantalum deposition from solutions in contact with carbonate-containing rocks (carbonatites), however, the extent of ore occurrences are incommensurable.

For the first time, using the mineral solubility method, the NaF concentrations were evaluated in L_1 and L_2 fluid phases in the immiscible region of H_2O-NaF system at 800°C and 230 MPa.

The authors are grateful to A.N. Nekrasov, V.K. Karandashev (IP RAS,) and O.L. Samokhvalova for research assistance. Financial support by RFBR, project 11-05-01185-a and ONZ program N2.

References:

1. Kotelnikova Z.A., A.R. Kotelnikov (2008). NaF-Bearing Fluids: Experimental investigation at 500–800°C and P = 2000 bar using synthetic fluid inclusions in quartz. *Geochem International*, No. 46, p. 48-61.
2. Peretyazko I.S. (2008). The properties of fluid inclusions with solutions of P-Q type. *RMS DPI* 208-1-30-0. P. 124-127. http://www.minsoc.ru/2008-1-30-0.
3. Prasad S. (1995). Electrometric studies of the formation of Niobates as a function of pH. *J. Braz. Chem. Soc.*, V.6, No. 1, p. 7-12.
4. Tytko K.H. (1999). A bond model for polyoxometalate ions composed MO_6 octahedra (Mok polyhedra with k>4). *A Bond Valence Approach.*, V. 93, p. 65-124.
5. Wood S.A. (2005). The aqueous geochemistry of zirconium, hafnium, niobium and tantalum. In Rare-Element Geochemistry and Mineral Deposits: Geological Association of Canada (Linnen, R.L. & Samson, I.M., eds.). *GAC Short Course Notes*, V. 17, p. 217-268.

Kotova N. P. Experimental study of temperature dependence of niobium oxide solubility in fluoride solutions in connection with genesis of tantalum deposits

Institute of experimental mineralogy RAS, Chernogolovka

Abstact. The dependence of Nb_2O_5 solubility as a function of temperature was investigated in HF, KF solutions with concentrations 0.1 and 1 m at 300, 400, 500 and 550 °C and 1000 bar under Co-CoO oxidizing conditions. The experimental data show that, for the range of temperatures and pressure (300 to 550 °C and 1000 bar) considered in this study, the solubility of Nb does not strongly depend on the T- conditions. The solubility and hydrothermal transfer of Nb are favored by concentrated F-bearing solutions under reducing conditions.

Key words: experiment, oxide niobium, hydrothermal solubility, fluoride solutions, temperature dependence.

Citation: Kotova N.P. (2013). Experimental study of temperature dependence of niobium oxide solubility in fluoride solutios in connection with genesisof tantalum deposits. Electron. Scien. - Inform. J. "Vestn. Otd. nauk Zemle RAN", No

The role problem of magmatic and hydrothermal-metasomatic factors in the formation of industrial concentration of tantalum in the granites is still a controversial. Additional criteria and restrictions for its solution can provide the results of experimental studies of the behavior of rare metals in granitic melts and aqueous fluids at temperatures and pressures corresponding to the conditions of formation of rare metal deposits.

We carried out a systematic experimental study on mineral solubility of stable under natural conditions, the mineral phases of tantalum-niobates (columbite, pyrochlore, etc.), as well as the simple oxides of Ta and Nb (Ta_2O_5 and Nb_2O_5) [Korzhinskaya, Kotova., 2012; Kotova., 2012]. It is related to the need to obtain quantitative assessments of the possibility of the hydrothermal transport and deposition of tantalum and niobium under the physical and chemical conditions typical for formation of the main types of endogenous deposits of these metals associated with "apogranite" pegmatites, alkaline metasomatic, alkali syenite and carbonatite. The study of the solubility of the simple oxides of Ta and Nb is an indispensable link in fundamental problem of the genesis of rare metal deposits of tantalum and niobium as a more complex composition of natural minerals with a lower solubility complicates thermodynamic interpretation of results.

In order to experimentally cover almost all the conditions of formation of tantalum-niobium deposits we continued experiments to determine the Nb_2O_5 solubility in fluoride aqueous solutions. The temperature dependence of niobium oxide solubility was investigated at T = 300, 400, 500 and 550° C, P = 1000 bar in the fluoride solutions of HF and KF at concentration of 0.1 and 1 m in the presence of oxygen buffer Co-CoO. A sealed-capsule quench technique was employed. Experiments were performed on high pressure hydrothermal apparatuses. The capsules and the container with buffer were sealed into cold-seal pressure vessel of Tuttle type with big working volume that gives possibility to isolate the capsules from the container with buffer. The same technique was used to study Ta_2O_5 solubility in fluoride and chloride solutions. Solid run products were separated from the solutions by centrifugation method. After that the quenched aqueous solutions were analyzed by ICP/MS (Inductively Coupled Plasma Mass Spectrometry) and ICP/AES (Atomic Emission Spectroscopy) procedures for Nb, Ta, Mn, and Fe and admixture elements: Ti, W, Sn, K, and Na. To control congruent or incongruent dissolution of Ta oxide and to determine chemical composition of newly-formed phases (in case of their manifestation) the initial materials and solid run products were studied by X-ray phase and micro-probe analysis method (Cam Scan MV2300(VE GA TS5130MM).

The experimental data show that in 0.1m HF the concentration of Ta changes very little with increasing temperature. It is around $10^{-2.}$ m for all temperatures considered. The exception is the data at T = 400° C, where the content of niobium is $10^{-3.5}$ m. In solutions of 1 m HF the weakly pronounced negative temperature dependence of the Nb_2O_5 solubility is observed. The highest Nb concentration ($10^{-}1$ m) was detected at T = 300° C, which is 0.5 orders of magnitude more than that obtained for other temperatures.

Nb_2O_5 solubility increases with increasing fluoride concentration (Fig. 1). At low temperatures (up to 400° C) the content of Nb in 1 m HF is 2 orders of magnitude more than that in 0.1 m HF. At high temperatures (above 400° C) it is 1 order more than that in 0.1 m HF.

In KF solutions, as in HF solutions, the weakly pronounced negative temperature dependence of the of niobium oxide solubility is observed (Fig. 2). The content of Nb in 1 m KF is 10^{-2} m, which is one order lower than in 1 m HF. The concentration of Nb in 0.1 m KF solutions is $10^{-2.5}$ m, similar to that seen in 0.1 m HF solutions. The exception is the data at T = 400° C, where the content of niobium in 1 m KF is 10-3 m and in 0,1 m KF -$10^{-3.5}$ m, which is 1 order of magnitude lower than that obtained for other temperatures.

The solubility of Nb_2O_5 as a function of the total concentrations of HF and KF is much stronger than the temperature dependence. The content of Nb in 1 m KF is 0.5 orders of magnitude more than that in 0.1 m KF over all temperatures considered.

According to our experimental data over all investigated range of temperatures in 0.1 m HF solutions niobium oxide dissolves congruently (without the composition changing). In 1 m KF solutions niobium oxide has an incongruent solubility. The crystals of niobium oxide fluoride with the formula Nb_3O_7F, belonging to the orthorhombic system, are formed.

In KF solutions over all investigated range of temperatures niobium oxide dissolves incongruently. In this case, at T = 300° C in 0.1 m KF solutions the synthetic pyrochlore Nb_2 (O, OH)$_6$ $1.5H_2O$ (cubic crystals) is formed , which is very similar to natural potassium pyrochlore $(K, H_2O)_2$ $(Nb, Ti)_{1.8}$ (O, OH)$_6$. At T = 400, 500 and 550° C niobium oxide is replaced by oxyfluoride of potassium type KNb_6O_{15}, belonging to the monoclinic crystal system. In 1m KF solution at all temperatures considered potassium- niobate $K_2NB_4O_{11}$ is formed, which belongs to the tetragonal system.

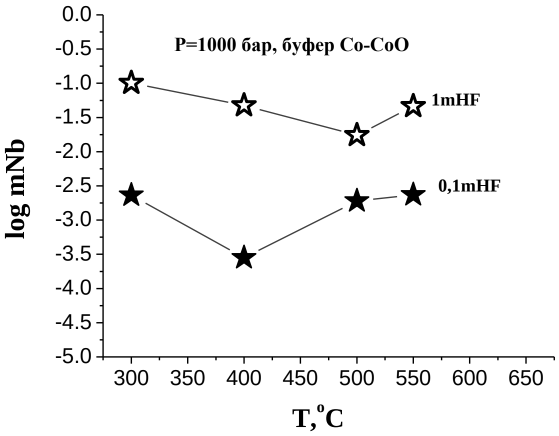

Fig. 1 The solubility of Nb_2O_5 as a function of T in HF solutions at P= 1 kbar (Co-CoO buffer)

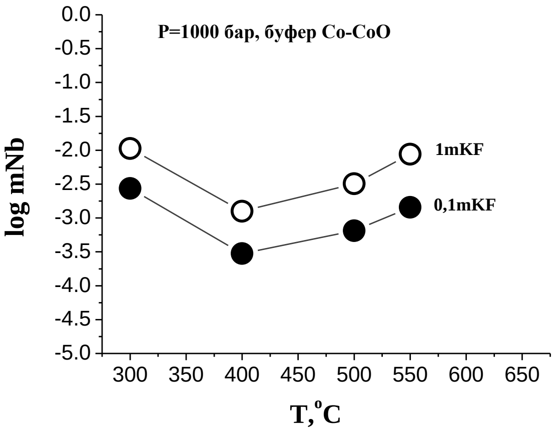

Fig. 2 The solubility of Nb_2O_5 as a function of T in KF solutions at P= 1 kbar (Co-CoO buffer)

The studies allow us to conclude that in fluoride solutions of various cationic composition (HF and KF) for the range of temperatures (300 to 550° C) considered in this study (Co-CoO buffer), the solubility of Nb does not strongly depend on the T conditions. At the same time, the concentration dependence of niobium oxide solubility is strong and positive.

Thus, these data provide a basis to assert that the solubility and hydrothermal transport of niobium are favored by concentrated F-bearing solutions under reducing conditions

Financial support by RFBR, project 11-05-01185-a and ONZ program N2

References:

1. Korzhinskaya V.S., N.P. Kotova (2012). Experimental modeling of possibility of hydrothermal transferring niobium by fluoride solutions. *Vestn. Otd. nauk Zemle,* 4, NZ9001, doi:10.2205/2012NZ_ASEMPG.
2. Kotova N.P. (2012). Experimental study of concentration dependence of niobium oxide solubility in fluoride solutions at T=550°C, P=500 bar and low oxygen fugacity (Co-CoO buffer). *Vestn. Otd. nauk Zemle*, 4, NZ9001, doi:10.2205/2012NZ_ASEMPG